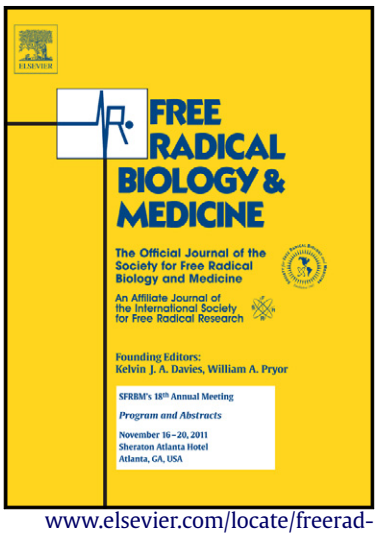

www.elsevier.com/locate/freerad-biomed

Redox metabolism in *trypanosoma cruzi*: functional characterization of tryparedoxins revisited

Diego G. Arias, Vanina E. Marquez, María L. Chiribao, Fernanda R. Gadelha, Carlos Robello, Alberto A. Iglesias, Sergio A. Guerrero

PII: S0891-5849(13)00205-0
DOI: http://dx.doi.org/10.1016/j.freeradbiomed.2013.04.036
Reference: FRB11545

To appear in: *Free Radical Biology and Medicine*

Received date: 14 August 2012
Revised date: 4 April 2013
Accepted date: 30 April 2013

Cite this article as: Diego G. Arias, Vanina E. Marquez, María L. Chiribao, Fernanda R. Gadelha, Carlos Robello, Alberto A. Iglesias, Sergio A. Guerrero, Redox metabolism in *trypanosoma cruzi*: functional characterization of tryparedoxins revisited, *Free Radical Biology and Medicine,* http://dx.doi.org/10.1016/j.freeradbiomed.2013.04.036

REDOX METABOLISM IN *TRYPANOSOMA CRUZI*: FUNCTIONAL CHARACTERIZATION OF TRYPAREDOXINS REVISITED

Diego G. Arias[1], Vanina E. Marquez[1], María L. Chiribao[2], Fernanda R. Gadelha[3], Carlos Robello[2], Alberto A. Iglesias[1], Sergio A. Guerrero[1]*

[1]Instituto de Agrobiotecnología del Litoral, Facultad de Bioquímica y Ciencias Biológicas, UNL-CONICET, Santa Fe, Argentina.

[2]Departamento de Bioquímica, Facultad de Medicina, Universidad de la República and Unidad de Biología Molecular, Instituto Pasteur Montevideo, Montevideo, Uruguay.

[3]Departamento de Bioquímica, Instituto de Biologia, Unicamp, Campinas, Brazil.

Corresponding Author: Sergio A. Guerrero, Laboratorio de Bioquímica Microbiana, IAL-CONICET, Facultad de Bioquímica y Ciencias Biológicas, Universidad Nacional del Litoral. Ciudad Universitaria - Paraje El Pozo, 3000 Santa Fe, Argentina. Tel: 54 342 457 5209 ext. 131. Email: sguerrer@fbcb.unl.edu.ar

ABSTRACT

Tryparedoxins (TXNs) are multipurpose oxidoreductases from trypanosomatids that transfer reducing equivalents from trypanothione to different thiol proteins. In *Trypanosoma cruzi,* two genes coding for TXN like proteins have been identified: TXNI, previously characterized as a cytoplasmic protein, and TXNII, a putative tail-anchored membrane protein. In this work, we performed a comparative functional characterization of *T. cruzi* TXNs. Particularly, we cloned the gene region coding for the soluble version of TXNII for its heterologous expression. The truncated recombinant protein (without its 22 C-terminal transmenbrane amino acids) showed TXN activity. It was also able to transfer reducing equivalents from trypanothione, glutathione or dihydrolipoamide to different acceptors, including methionine sulfoxide reductases and peroxiredoxins. Results support the occurrence and functionality of a second tryparedoxin, which appears as a new component in redox scenario in *T. cruzi*.

Keywords: Trypanosoma; Tryparedoxin; Trypanothione; ROS.

Abbreviations: Grx, glutaredoxin; GR, glutathione reductase; TR, trypanothione reductase; $T(SH)_2$, trypanothione; TS_2, trypanothione disulfide; GSSG, glutathione disulfide; GSH, reduced glutathione; TXNPx, 2-Cys-peroxiredoxin-type tryparedoxin peroxidase; GPxI, glutathione peroxidase-type tryparedoxin peroxidase I; LipDH, lipoamide dehydrogenase; HEDS, hydroxyethyl disulfide; GspSH, reduced glutathionylspermidine; TXN, tryparedoxin; TRX, thioredoxin; CySSyC, cystine; βME, β-mercaptoethanol; DTT, dithiotreytol; *t*-bOOH, *tert*-butyl hydroperoxide; L-Met(*S*)SO, L-methionine-*S*-sulfoxide; MSRA, methionine sulfoxide reductase A, APx: ascorbate peroxidase.

INTRODUCTION

Trypanosomatids are unicellular organisms of the order Kinetoplastida that parasitize a wide variety of invertebrate and vertebrate hosts [1]. The most relevant specimens for human and animal health belong to the genera *Trypanosoma* and *Leishmania*, which annually affect half a million people around the world (WHO; http://www.who.int/en/). *Trypanosoma cruzi* is the etiologic agent of Chagas' disease, an infection that affects several million people in Latin America [2, 3]. Tryparedoxins (TXNs) are low molecular mass dithiol proteins in trypanosomatids [1, 2]. They represent a distinctive molecular group within the thioredoxin (TRX) oxidoreductase superfamily, which is characterized by a WCPPC motif at their catalytic center [4, 5]. Despite the low sequence similarity, which is restricted to the active site region and a few other adjacent amino acid residues, TXNs and TRXs have the same core structure: a five-stranded β-sheet surrounded by four α-helices [6, 7]. An insertion of 24 to 36 residues between domains α-2 and ß-5 is responsible for the substantially larger size of TXNs (16 kDa) in comparison to TRXs (12 kDa) [7, 8]. The N-terminal cysteine of the CPPC active site motif is exposed to the solvent. Its nucleophilicity is warranted by a fast proton shuttling involving the second cysteine and a network of uncharged internal residues [8-10]. The thiolate anion reacts with disulfides from specific proteins leading to mixed disulfides between TXN and the respective target molecule. Attack of this mixed disulfide by the vicinal Cys of TXN releases the reduced target protein and oxidizes TXN [9-11].

TXNs are reduced by trypanothione [N^1,N^8-bis(glutathionyl) spermidine or $T(SH)_2$], a low molecular mass dithiol found almost exclusively in trypanosomatids. It is maintained in its reduced form by a flavoprotein, the trypanothione reductase (TR), at the expense of

NADPH [4, 7, 9]. The $T(SH)_2$/TXN system delivers electrons for the detoxification of hydroperoxides, and reduction of ribonucleotides, peroxynitrite, and methionine sulfoxide, as well as for other cellular processes regulated by thiol/disulfide exchanges [12-18]. Various experimental data have shown the relevance of TXN for the survival of trypanosomatids, making the protein a potential target candidate for drug design [1, 2]. In *Trypanosoma brucei*, down-regulation of TXN expression impairs the antioxidant metabolism affecting the cell growth [19]. Moreover, gene knockout assays performed in *Leishmania infantum*, demonstrated that TXNI is essential in this parasite [20].

Cytosolic TXN has been identified in different trypanosomatids [2]. In *L. infantum*, a soluble TXN (named TXNII) has been experimentally detected in the mitochondrion [12, 21], and a gene coding for a TXNIII has been identified from its genome. Biochemical studies have characterized TXNIII as a tail-anchored mitochondrial outer membrane protein that is unable to reduce sulfur-containing peroxidases [22]. In *T. cruzi*, two genes coding for TXN have been identified, but only the cytosolic isoform (TXNI) was functionally characterized [1, 17, 23]. The other isoform (*Tcr*TXNII), differs from TXNI in having a central insertion and an extra C-terminal tail of 15 and 26 amino acids, respectively [1, 17]. In this work, we expressed a recombinant soluble version of *Tcr*TXNII, truncated at the C-term, to characterize the kinetic and thermodynamic properties of the protein. Results are discussed including a comparative analysis between the properties of TXNI and TXNII, establishing different functional roles for the proteins in the redox metabolism of *T. cruzi*, and considering the presence of a second functional tryparedoxin in the parasite.

MATERIALS AND METHODS

Materials

Bacteriological media were purchased from Britania Laboratories (Argentina), *Taq* DNA polymerase and restriction enzymes were purchased from Promega (Argentina), while trypanothione disulfide and glutathionyl-spermidine disulfide were acquired from Bachem (USA). All other reagents and chemicals were of the highest quality commercially available from Sigma-Aldrich (Argentina) or similar.

Protozoa and culture procedure

T. cruzi CL-Brener epimastigote cells were cultivated axenically at 28 ºC in LIT media supplemented with 10 % (w/v) bovine fetal serum and 20 $\mu g \cdot ml^{-1}$ hemin, as previously reported [24]. Metacyclic trypomastigotes were obtained from axenic cultures under differentiating conditions [25] and amastigotes were recovered from cultures of Vero cells infected with trypomastigotes [26].

Bacteria and plasmids

Escherichia coli Top 10 F´ and *E. coli* BL21 (DE3) cells (Invitrogen, Argentina) were utilized in routine plasmid construction and protein expression assays, respectively. The vector pGEM-T Easy (Promega, Argentina) was selected for cloning and sequencing purposes, with pET-28c (Novagen, Argentina) used as the expression vector. DNA manipulation, *E. coli* culture, and transformation were performed according to standard protocols [27].

Molecular cloning of the tcrtxnII *gene*

Genomic DNA was obtained from epimastigote cells as previously described [27]. The *tcrtxnII* gene was amplified from *T. cruzi* CL-Brener genomic DNA by PCR, using oligonucleotides designed based on information obtained from spliced sequences data base (Wellcome Trust, Pathogen Sequencing Unit, (http://www.genedb.org/): TcrTXNIIFo:5´-GCTAGCGGATCCATGCTGCCACGCGTACTTGGGG-3´; TcrTXNIIRev: 5´-AAGCTTTCACCGCCAGAATTGATACA-3´ and TcrTXNIIΔ22CRev: 5´-AAGCTTTTACCTCAGTCCTTCACCGTCTG-3´. The PCR products were purified and ligated into the pGEM-T Easy cloning vector (Promega, Argentina) to facilitate further work. Fidelity and correctness of each gene were confirmed on both strands by complete sequencing (Macrogen, South Korea).

Generation of expression vectors

pGEM-T Easy plasmids containing the cloned genes and the vector pET28c (Novagen, Argentina) were digested with *Nhe*I and *Hind*III. Ligation to pET28c vector was performed using T4 DNA ligase at 16 °C during 16 h. Competent *E. coli* BL21 (DE3) cells were transformed with the respective construct and selected on agar plates containing Lysogeny Broth (LB; 10 $g \cdot l^{-1}$ NaCl, 5 $g \cdot l^{-1}$ yeast extract, 10 $g \cdot l^{-1}$ peptone, pH 7.4) supplemented with kanamycin (50 $\mu g \cdot ml^{-1}$).

Overexpression and purification of recombinant proteins

Single colonies of *E. coli* BL21 (DE3) transformed with the respective recombinant plasmid were selected. Overnight cultures were diluted 1/100 in fresh medium (LB broth supplemented with 50 $\mu g \cdot ml^{-1}$ kanamycin) and grown under identical conditions to exponential phase, OD_{600} 0.6. The expression of the recombinant protein was induced with 0.5 mM IPTG (final concentration), followed by orbital shaking at 20 °C. After 16 h, cells were harvested and stored at −20 °C. Purification of each recombinant protein was performed using a Ni^{2+}–Hi-Trap resin (GE-Healthcare, Argentina). Briefly, the bacterial pellet was resuspended in binding buffer (20 mM Tris–HCl, pH 7.5, 400 mM NaCl and 10 mM imidazole) and disrupted by sonication. The lysate was centrifuged (10,000 x g, 30 min) to remove cell debris. The resultant crude extract was loaded onto a column equilibrated with binding buffer. After washing with 10 bead volumes of binding buffer, the recombinant protein was removed from the column with elution buffer (20 mM Tris–HCl, pH 7.5, 400 mM NaCl, 300 mM imidazole). Pure enzyme fractions were pooled, concentrated by ultrafiltration, and stored at -80 °C in 20 mM Tris–HCl, pH 7.5; 1 mM EDTA and 5% (v/v) glycerol. Under the specified storage conditions, the recombinant proteins were stable for, at least, 12 months. *Tcr*TXNI, *Tcr*TR, *Tcr*cTXNPx, *Tcr*mTXNPx, *Tcr*GPxI, *Tcr*TRX and *Tcr*MSRA were obtained according to previous reports [13, 15, 17, 18, 28-30].

Protein methods

Cell-free extracts were analyzed by SDS–PAGE [31] and protein contents were determined by the method of Bradford [32], with BSA as standard. Serum anti-*Tcr*TXNIIΔ22C was

prepared by rabbit immunization with the purified recombinant proteins according to Vaitukaitis et al [33].

T. cruzi protein extracts (40 μg) were analyzed by SDS-PAGE under reducing conditions and blotted to a nitrocellulose membrane (GE Healthcare, Argentina). Membranes were blocked for 1 h in 5% (w/v) skimmed milk in PBS buffer (8 $g \cdot l^{-1}$ NaCl, 0.2 $g \cdot l^{-1}$ KCl, 1.44 $g \cdot l^{-1}$ Na_2HPO_4, 0.24 $g \cdot l^{-1}$ KH_2PO_4, pH 7.4), washed with PBS-Tween 20 0.05% (v/v), and incubated with TXNII antibody diluted 1/1000 in PBS-BSA 1% (w/v) for 16 h at 4 °C. After three washes, membranes were incubated with goat anti rabbit-IgG conjugated to FITC (Thermo Scientific, Argentina). Signal recognition was performed with Typhoon 9400 (GE Healthcare, Argentina).

Determination of the molecular mass by gel filtration chromatography

The estimation of the molecular size of native *Tcr*TXNIIΔ22C was performed in a Superdex 200 (GE-Healthcare, Argentina) column equilibrated with 25 mM Tris–HCl, pH 7.5, 1 mM EDTA and 100 mM NaCl. The purified protein was analyzed chromatografically together with different molecular mass standards (GE-Healthcare, Argentina): bovine serum albumin, 66 kDa; ovalbumin, 43 kDa; carbonic anhydrase, 29 kDa; and lysozyme, 14 kDa.

Tryparedoxin activity assays

Enzymatic activities were measured by monitoring NADPH oxidation at 340 nm by means of a coupled assay that guarantees the regeneration of reduced *Tcr*TXNs. All enzymatic assays were performed spectrophotometrically at 30 °C using a Multiskan Ascent one-channel vertical light path filter photometer (Thermo Electron Co.). The general assay medium contained 100 mM Tris–HCl, pH 7.5, and 2 mM EDTA and 300 μM NADPH over which specific additions were made for each of the enzymes. In all the cases, the final volume was of 50 μl.

Tryparedoxin activity of *Tcr*TXNI or *Tcr*TXNIIΔ22C was determined by means of a *Tcr*cTXNPx-dependent *t*-bOOH reduction assay [5, 34], using GSH (15-5000 μM), $T(SH)_2$ (3-100 μM), GSP-SH (3-200 μM) or dihydrolipoamide (3-200 μM) as reducing agent and different concentrations of *Tcr*TXNs (0.25-2 μM).

$T(SH)_2$-dependent reduction of GSSG, CySSyC or *S*-nitrosothiols by *Tcr*TXNs was performed in a reaction mixture containing 100 μM TS_2, 1 μM *Tcr*TR, 15-1000 μM GSSG, CySSyC, GSNO or CySNO and different concentrations (0.5-12 μM) of both *Tcr*TXNI and *Tcr*TXNIIΔ22C.

The ability of *Tcr*TXNs for transferring electrons to physiological thiol-dependent peroxidases like *Tcr*cTXNPx, *Tcr*mTXNPx and *Tcr*GPxI, was determined by measuring the reduction of *t*-bOOH [35]. The reaction mixture contained 100 μM TS_2, 1 μM *Tcr*TR, different concentrations of *Tcr*TXNI or *Tcr*TXNIIΔ22C (0.25-20 μM) and 0.1-5 μM of peroxidases (either *Tcr*cTXNPx, *Tcr*mTXNPx, or *Tcr*GPxI). Reactions began after addition of 70 μM *t*-bOOH.

The capacity of *Tcr*TXNs for transferring electrons to *Tcr*MSRAs was determined by measuring the L-Met(*S*)SO reduction [18]. The reaction mixture contained 100 μM TS_2, 1 μM *Tcr*TR, 0.1-5 μM *Tcr*MSRAs and different concentrations (0.25-20 μM) of *Tcr*TXNI or *Tcr*TXNIIΔ22C. Reactions began after addition of 2.5 mM L-Met(*S*)SO.

GSH-dependent reduction of dehydro-ascorbate (DHA) by *Tcr*TXNs was performed in a reaction mix containing 3 mM GSH, 1 $U \cdot ml^{-1}$ yeast GR, 15-1000 μM DHA and different concentrations (0.25-20 μM) of *Tcr*TXNI or *Tcr*TXNIIΔ22C.

$T(SH)_2$-dependent reduction of *Tcr*TRX by *Tcr*TXNs was performed in a reaction mix containing 100 μM TS_2, 1μM *Tcr*TR, 0.5-20 μM *Tcr*TRX, 0.25-1 μM *Tcr*TXNI or 0.5-20 μM *Tcr*TXNIIΔ22C and 130 μM bovine insulin as final electron acceptor.

Kinetic constants were determined by fitting the data with a nonlinear least-squares formula and the Michaelis-Menten hyperbolic equation using the program Origin™ 7.0. Kinetic constants are the mean of at least three independent sets of data, and they are reproducible within ±10%.

Glutathione-TXN redox equilibrium

Redox equilibrium assays were carried out incubating the oxidized proteins (125 to 500 μM) for 4 h at 30 ºC in a reaction mixture containing 100 mM Tris–HCl, pH 7.5, 2 mM EDTA and 1 mM GSH. After incubation, 5% (w/v) TCA was added to separate proteins from the reaction mixture. The GSSG generated was determined by a kinetic method based

on the NADPH-dependent reduction of GSSG by GR, using a GSSG calibration curve. GSH concentration at the equilibrium was estimated using DTNB reagent [36]. The reduced and oxidized fractions of TXNs were estimated analyzing ratios of GSH:GSSG. With these data, the equilibrium constants for TXN-reduction by GSH were estimated. Standard reduction potentials ($E_{m7.5}$) were also determined by means of the Nernst equation [37]. An $E^{o}_{7.5\ GSSG/GSH}$ of -270 mV was used for all calculations [38].

Redox titration for determining TcrTXNPxs and TcrGPxI standard reduction potential

Redox titrations were carried out by incubation of the proteins (1-2 μM) for 4 h at 30 ºC in a reaction mixture containing 200 mM Tris–HCl, pH 7.5, 2 mM EDTA and variable molar ratios of GSH/GSSG or βME/HEDS to reach different half-cell potentials (E_h, from -340 to -40 mV) according to the Nernst equation. Afterward, samples were analyzed by non-reducing SDS-PAGE and the abundance of reduced fractions was estimated by densitometry, using the program LabImage 2.7.2 (Kapelan GMBH). Titration curves were fitted as reduced fraction versus E_h. Standard reduction potentials ($E_{m7.5}$) were determined by means of nonlinear regression of the data according to logistic model using the program Origin 7.0.™ [18].

Measurement of the thiolate anion by UV absorption

The pH-dependent cysteine ionization was followed by the absorption of the thiolate anion at 240 nm [10, 39]. Spectra of either oxidized or reduced (after incubation with 10 mM DTT for 10 min at room temperature) 8–10 μM of both *Tcr*TXNI and *Tcr*TXNIIΔ22C, were recorded between 200 and 340 nm. The proteins were analyzed at 25 °C in 1 ml of the reaction media containing 100 mM MES-NaOH (pH 5.0 to 6.0) or MOPS-NaOH (pH 6.0 to 8.5) and glycine-NaOH (pH 8.5 to 10.5). The spectra were measured against buffer solution in a stoppered quartz cuvette in a Boeco S-22 UV-Vis spectrophotometer and the absorbance was converted into molar extinction coefficient. For a single thiolate group a value between 4 and 6 $mM^{-1}\ cm^{-1}$ was used, according to previous reports [40].

Extraction of vesicular and membrane proteins

T. cruzi epimastigotes ($5 \cdot 10^8$ cells) were pelleted and suspended in 1 ml of 10 mM Tris-HCl pH 7.5, 1 mM EDTA (plus cocktail of protease inhibitors) and disrupted by sonication. The lysate was sedimented by centrifugation for 60 min at 14,000×*g*. The soluble and insoluble fractions were treated with 8 mM $CaCl_2$ (for vesicles and microsomes precipitation [41]) and 0.1 M Na_2CO_3 pH 11.0, respectively. After incubation for 30 min at 4 °C, the samples were centrifuged for 30 min at 14,000×*g*. Soluble and insoluble fractions obtained in both procedures were analyzed by western blot using specific polyclonal sera against *Tcr*TXNII (diluted 1/1000) or *Tcr*TXNI (diluted 1/2000).

Digitonin treatment of T. cruzi *epimastigote*

Differential membrane permeabilization was performed as described by Ceylan et al. [42]. About $5 \cdot 10^8$ epimastigote cells were washed once with PBS and twice with 20 mM Tris-HCl, 100 mM NaCl, 1 mM EDTA and 2% (w/v) glucose, pH 7.5. A stock solution of 20 mg/ml digitonin (Sigma Aldrich) was prepared in water and various concentrations were made by dilution with buffer. For every extraction step, digitonin dilution was added to the cell pellet (100 µl each $1 \cdot 10^7$ cells), incubated at 30 °C for 5 min, and centrifuged at 10,000 x g and 4° C for 5 min. Supernatants were mixed with SDS-PAGE sample buffer, boiled for 5 min and stored at -20 °C. Aliquots were analyzed by western blot using specific polyclonal sera designed in rabbit against different cellular targets like *Tcr*TXNII (diluted 1/1000) or *Tcr*cTXNPx (diluted 1/1000) or *Tcr*mTXNPx (diluted 1/1000) or *Triticum aestivum* glyceraldehyde-3-phosphate dehydrogenase (GAPDH) (diluted 1/500) or *Tbr*CytC (diluted 1/500) or *Tbr*BIP (diluted 1/1000). FITC-conjugated goat anti-rabbit (diluted 1/10000) was used as secondary antibody (Thermo Scientific). Signal recognition was performed with Typhoon™ 9400 (GE Healthcare).

Digitonin extraction and proteinase K protection assay

About $5 \cdot 10^8$ epimastigote cells were suspended with 20 mM Tris-HCl, 100 mM NaCl, 1 mM EDTA, 2% (w/v) glucose, pH 7.5 and 5 $\mu g \cdot ml^{-1}$ proteinase K. For each extraction/digestion step, a digitonin dilution (0-4 $mg \cdot ml^{-1}$) was added to the cell pellets (100 µl each $1 \cdot 10^7$ epimastigote cells) and incubated at 37 °C for 15 min. To inhibit

proteinase K reaction, 100 mM phenylmethylsulfonyl fluoride (PMSF) was added to all samples. Proteins were analyzed by western blot using specific polyclonal sera against *Tcr*TXNII (diluted 1/1000), *Tcr*cTXNPx (diluted 1/2000), *Tbr*CytC (diluted 1/1000), *Tbr*BIP (diluted 1/2000) or *Tcr*APx (diluted 1/2000).

Indirect immunofluorescence

For indirect immunofluorescence (IIF) assays, epimastigotes, trypomastigotes or infected Vero cells were washed twice with cold PBS. Trypomastigotes and epimastigotes were fixed with paraformaldehyde 4% (w/v) in PBS for 20 min at room temperature, infected Vero cells were fixed and permeabilized with cold ethanol for 10 min. After fixation, epimastigotes and trypomastigotes were allowed to adhere to slides for 30 min at 37 ºC and then permeabilized 10 min with 0.2% (v/v) Triton-X100 in PBS 1X. At room temperature the parasites were blocked with 2% (w/v) BSA during 1 h, washed twice with PBS 1X 0.1% (v/v) Tween-20 and incubated for 2 h with purified anti TXNII antisera diluted 1/200 in PBS 1X 1% (w/v) BSA and 0.1% (v/v) Tween-20. After three washes the slides were stained with ALEXA 488-conjugated goat anti-rabbit immunoglobulin G at 1/1000 dilution. After three washes the slides were incubated for 5 min with TO-PRO®-3 (Invitrogen) diluted 1/500 in PBS. After three washes, slides were mounted with ProLong Antifade (Invitrogen) and visualized under a confocal microscope.

RESULTS

Molecular cloning and recombinant expression of tcrtxnii *gene from* T. cruzi

The *T. cruzi* genome database contains 2 putative *txn* genes: one corresponding to the previously characterized *tcrtxni* gene [23], and a second predicted *txn* coding sequence (GenID: Tc00.1047053509997.20, *tcrtxnii*), previously analyzed by Wilkinson et al [17]. We amplified *tcrtxnii* from genomic DNA of *T. cruzi* (CL-Brener) and cloned it into the pGEM-T Easy vector for analysis. The *tcrtxnii* encodes a protein with a theoretical molecular mass of 21.9 kDa and a *p*I of 8.64. Figure 1 shows the *Tcr*TXNII predicted amino acid sequence and compares it to other TXNs. *Tcr*TXNII has an insertion of 15 amino acids in the central core and a C-terminus extension (22 amino acids long) enriched in hydrophobic residues (see Figure 1). *In silico* analysis predicts as a transmembrane

domain this hydrophobic C-terminus extension (using SOSUI, TopPred and TMpred servers). These attributes in the sequence distinguish *Tcr*TXNII from other TXNs previously characterized.

With the aim of characterizing the functionality of *Tcr*TXNII, the entire protein was expressed in bacteria as a fusion protein with an N-terminal His-tag for chromatographic purification. By the latter procedure the protein was expressed as inclusion bodies (data not shown). In order to maximize the soluble expression of functional *Tcr*TXNII, we performed a truncated version of the protein (lacking the C-terminal 22 amino acids, *Tcr*TXNIIΔ22C, Supplemental data - Figure 1). All the *in vitro* experiments were performed with this truncated version of TXNII.

Tcr*TXNIIΔ22C presented trypanothione-dependent oxidoreductase activity*

We tested the parasite protein ability to catalyze the reduction of bovine insulin by $T(SH)_2$, following NADPH oxidation in the presence of TR. Figure 2 shows that *Tcr*TXNIIΔ22C was able to accept reduction equivalents from $T(SH)_2$ with a moderated enzymatic capacity, between *Tcr*TXNI and *Tcr*TRX ($k_{cat\ app}$ calculated in 2.3 ± 0.1 min^{-1}, 9.3 ± 0.5 min^{-1} and 0.20 ± 0.03 min^{-1} for *Tcr*TXNIIΔ22C, *Tcr*TXNI, and *Tcr*TRX, respectively).

Enzymatic assays indicated that *Tcr*TXNIIΔ22C was active for transferring reducing equivalents to cytoplasmatic (*Tcr*cTXNPx), mitochondrial (*Tcr*mTXNPx) 2-Cys peroxiredoxins, and glutathione peroxidase I (*Tcr*GPxI). This was evaluated by the coupled assay for trypanothione-dependent *t*-bOOH reduction via a tryparedoxin/peroxidase-mediated reaction (Figure 3-A). Our findings differ from those previously reported for *Leishmania infantum* TXNIII as this protein, homologue to *Tcr*TXNIIΔ22C, did not exhibit TXN activity in a similar assay [22]. Steady state kinetics revealed that under our experimental conditions *T. cruzi* TXNs reduced three trypanosomal thiol-dependent peroxidases with a hyperbolic behavior (Figure 3-A). Both *Tcr*TXNI and *Tcr*TXNIIΔ22C reduced *Tcr*cTXNPx with similar catalytic efficiencies. For *Tcr*mTXNPx and *Tcr*GPxI, reduction, *Tcr*TXNI showed second order kinetic constants one order of magnitude higher

than those of *Tcr*TXNIIΔ22C (Table 1). Results strongly support the functionality of *Tcr*TXNII as a true TXN, thus indicating its possible involvement in, for example, hydroperoxides detoxification pathway. Based on previous data about the participation of *Tcr*TXNI in the MSRA-dependent reduction of L-Met(*S*)SO [18] we evaluated the ability of *Tcr*MSRAs to use *Tcr*TXNIIΔ22C as a reducing substrate. As shown in Figure 3-B, the truncated protein was able to transfer reducing equivalents to *Tcr*MSRAs. Despite it showed a lower reduction efficiency in respect to that of *Tcr*TXNI, results suggest the possible role for *Tcr*TXNII in the pathway for repairing oxidized proteins. Table 1 shows a comparative analysis of the kinetic parameters obtained for *T. cruzi* Prxs, GPx and MSRAs reduction by *Tcr*TXNIIΔ22C and *Tcr*TXNI.

Tcr*TXNI and* Tcr*TXNII can use different low molecular mass thiols as reducing substrates*

We studied the capacity of *Tcr*TXNI and *Tcr*TXNII to use different low molecular mass thiols such as GSH, glutathionyl-spermidine (GSP-SH), and the dithiol dihydrolipoamide as a source of reducing equivalents (see results in Table 2). In fact, we detected that the oxidation rate of NAD(P)H was directly proportional to the thiol and TXN concentration, thus indicating that *Tcr*TXNs catalyze thiol oxidation. In relation to dithiol substrates, previous reports indicate that reduction of *Tcr*TXNs by $T(SH)_2$ (or less efficiently by dihydrolipoamide) followed second-order kinetics [4, 12]. To evaluate the catalytic behavior of *Tcr*TXNs reduction by thiol compounds, the second order rate constant for this reaction (k') was calculated according to the following equation:

$$v = k' \cdot [TXN_{Ox}] \cdot [R(SH)_2]$$

Thus, second order rate constants for TXN-reduction by dihydrolipoamide of $1.1 \cdot 10^3$ $M^{-1} \cdot s^{-1}$ and $3.8 \cdot 10^2$ $M^{-1} \cdot s^{-1}$ were obtained for *Tcr*TXNI and *Tcr*TXNIIΔ22C, respectively. The latter constants are about 10-fold lower than those determined using $T(SH)_2$ as reducing intermediate ($7.3 \cdot 10^4$ $M^{-1} \cdot s^{-1}$ for *Tcr*TXNI and $2.4 \cdot 10^3$ $M^{-1} \cdot s^{-1}$ for *Tcr*TXNIIΔ22C).

Contrarily, partial third-order kinetics was observed for reduction of *Tcr*TXNs by monothiols such as GSH or GSP-SH. According to the available literature on other

members of the TRX-family [43], monothiol oxidation to the respective disulfide by oxidized TXNs requires two consecutive reactions, the formation of a TXN-SSR mixed disulfide and the subsequent reaction between the mixed disulfide and RSH:

$$\mathrm{TXN\text{-}S_2} \underset{k2}{\overset{k1\cdot[\mathrm{RSH}]}{\rightleftarrows}} \mathrm{TXN-SSR} \underset{k4\cdot[\mathrm{RSSR}]}{\overset{k3\cdot[\mathrm{RSH}]}{\rightleftarrows}} \mathrm{TXN-(SH)_2}$$

Initial velocities were determined at various GSH or GSP-SH concentrations. At low concentrations of these monothiols (RSH), the reduction of TXNs followed second-order kinetics with respect to RSH concentration (Figure 4).

Based on literature [43], such dependence on second order-kinetics requires that: (*i)* the reaction of RSH with the active site disulfide is at equilibrium (k_2/k_3 >> [RSH]); (*ii*) the TXN-active site disulfide is not fully converted to the mixed disulfide, and (*iii*) the rate-limiting step is the reaction between the TXN-SSR mixed disulfide with RSH (k_3). For both *Tcr*TXNs, increasing GSH concentrations (above 0.15 mM) generated a change in the rate-determining step, producing a dependence on first-order kinetics. Under these conditions, the rate-determining step is the initial attack of GSH on TXN-S_2 (Figure 4). In this case, the reaction changes from second-order to first-order against GSH concentration. Data were fitted to the total kinetic model [43], including the potential for a change in rate-limiting step:

$$v = \frac{k_1 \cdot k_3 \cdot [\mathrm{TXN_{Ox}}] \cdot [\mathrm{RSH}]^2}{k_2 + k_3 \cdot [\mathrm{RSH}]}$$

Under conditions where [RSH] << k_2/k_3, the third-order rate constant for reduction of *Tcr*TXNs, namely k'' is equal to k_1k_3/k_2. Values of k'' calculated under these conditions are shown in Table 2. There was no evidence for a change in the rate-limiting step at the experimentally accessible concentrations of GSP-SH for *Tcr*TXNIIΔ22C (Supplemental data- Figure 2). These results would indicate that the reaction of GSP-SH with the *Tcr*TXNIIΔ22C-SS-GSP mixed disulfide (k_3) is faster than its reaction with *Tcr*TXNIIΔ22C-S_2 (k_1). It is interesting to point out that such a change in the rate-limiting step was observed during the *Tcr*TXNI-reduction with GSP-SH (Supplemental data – Figure 2). This kinetic model had been previously described for the GSH-dependent reduction of Grx and protein disulfide isomerase (PDI) [43, 44], with kinetic constants

supporting similar efficiency for either *Tcr*TXNI or *Tcr*TXNIIΔ22C in the use of GSH as reducing substrate. Conversely, *Tcr*TXNIIΔ22C showed less efficiency to oxidize GSP-SH than GSH, as deducted from kinetic parameters detailed in Table 2. This result defies the view that $T(SH)_2$ is the unique reductant for TXNs, adding new information about the relevance of GSH, GSP-SH and lipoamide in *T. cruzi* redox metabolism.

Reduction of non-protein substrates by TXNs

TXN-dependent reduction of non-protein disulfides, such as GSSG and CySSyC, were followed using a coupled assay system (see Materials and Methods). Second-order rate constants (k') summarized in Table 3 indicate that reduced *Tcr*TXNI or *Tcr*TXNIIΔ22C exhibited a capacity to reduce GSSG one order of magnitude higher than CySSyC. Besides, second order rate constants for GSSG-reduction by *Tcr*TXNs (Table 3) were about 100-1000 times higher than the one calculated for $T(SH)_2$-dependent GSSG reduction (10 $M^{-1}\cdot s^{-1}$ at pH 7.5 and 30 ºC). Results envisage a functional role of these proteins in the maintenance of glutathione in its reduced state. The functionality of a system using $T(SH)_2$ as an electron donor for *Tcr*TXNs to reduce GSSG acquires relevance because of the absence of glutathione reductase in trypanosomatids [2].

*Tcr*TXNs also exhibited GSH-dependent DHA reductase activity (typical activity of Grxs). The reaction was followed by measuring the NADPH-oxidation by means of a coupled enzymatic assay in the presence of GR, GSH, *Tcr*TXNs and DHA. Both *Tcr*TXNI and *Tcr*TXNIIΔ22C reduced DHA with similar catalytic efficiencies (~0.5-1.0·10^3 $M^{-1}\cdot s^{-1}$). As previously shown [45], $T(SH)_2$ reduces DHA with a second order rate constant of 22 $M^{-1}\cdot s^{-1}$ (at pH 6.5), which is three-order of magnitude faster than the reduction by GSH [45]. Thus, our results strongly support the GSH-dependent pathway for DHA reduction by *Tcr*TXNs as an alternative pathway for keeping ascorbate under its reduced form. In addition, the second-order rate constant values we obtained for GSSG, CySSyC and DHA reduction by *Tcr*TXNs are similar to those reported for TXNs from *T. brucei* and *Crithidia fasciculata* [4, 10].

Moreover, we investigated the ability of *T. cruzi* TXNs to reduce *S*-nitrosyl derivatives such as GSNO and CySNO. In the absence of *Tcr*TXNs these *S*-nitrosothiols can directly react with $T(SH)_2$ but at smaller rates (k'_{GSNO} = 2 $M^{-1}\cdot s^{-1}$ and k'_{CySNO} = 0.8 $M^{-1}\cdot s^{-1}$, at pH 7.5

and 30 ºC) than in the presence of either *Tcr*TXNI or *Tcr*TXNIIΔ22C in the reaction mixture (Supplemental data - Figure 3). Therefore, we point out that both redox intermediates behave as possible electron acceptor substrates for TXNs (see kinetic constants in Table 3).

TcrTXNI is more efficient than trypanothione in TRX reduction

In trypanosomatids, $T(SH)_2$ is considered the reducing substrate for TRX [39]. In view of the existence of previous reports for redoxin-redoxin interaction [34, 46], we evaluated the interplay between *Tcr*TXNs and *Tcr*TRX by means of a coupled assay using $T(SH)_2$ (via NADPH dependent reduction) as electron donor substrate, and bovine insulin as the final acceptor [29]. Figure 5 shows that in the presence of NADPH, *Tcr*TR, $T(SH)_2$, bovine insulin and variable *Tcr*TXNI and *Tcr*TRX concentrations, the rate of NADPH oxidation (or insulin precipitation) was increased proportionally. This supports a "synergy"-like phenomenon in the reducing equivalent flux due to a putative *Tcr*TXNI/*Tcr*TRX interaction. The latter was not observed when *Tcr*TXNI was replaced by *Tcr*TXNIIΔ22C, even at concentrations 20-fold higher (data no shown). Results indicate that, *in vivo,* *Tcr*TXNI would be a better reducing substrate for *Tcr*TRX than $T(SH)_2$. This is supported by second-order constant values calculated for *Tcr*TRX-reduction by these compounds ($k'_{T(SH)2} = 11\ M^{-1}\cdot s^{-1}$ versus $k'_{TcrTXNI} = 2.3 \cdot 10^5\ M^{-1}\cdot s^{-1}$) and the cytoplasmatic localization of both proteins [29, 47]. When bovine insulin was replaced by *Tcr*cTXNPx or *Tcr*mTXNPx (plus *t*-bOOH), the "synergy" in the reducing equivalent flux was not observed (data not shown).

Physical properties and reduction potential of TcrTXNs

The purified recombinant *Tcr*TXNIIΔ22C eluted as a protein of 22 kDa in gel-filtration chromatography either in the presence or absence of 10 mM DTT, thus revealing that the native protein has a monomeric structure (data no shown). This result agrees with molecular properties previously reported for *Tcr*TXNI [17] and other TXNs from other sources [4, 10].

Redox potentials of *Tcr*TXNs were determined using a method based in the equilibrium with GSH. Measurements were carried out at 30 °C and pH 7.5. Different ratios of oxidized

*Tcr*TXNI or *Tcr*TXNIIΔ22C with GSH were reached at the equilibrium after 4 h. Afterwards redox potentials of *T. cruzi* TXNs were calculated from the Nernst equation:

$$E^{o}_{7.5\ TXN} = E^{o}_{7.5\ GSSG/GSH} + \frac{R \cdot T}{z \cdot F} \cdot \ln\left(\frac{[TXN_{Re}] \cdot [GSSG]}{[TXN_{Ox}] \cdot [GSH]^2}\right)$$

Analysis of different reaction mixtures resulted in a standard redox potential at pH 7.5 of −235 ± 7 mV for *Tcr*TXNI and −227 ± 4 mV for *Tcr*TXNIIΔ22C.

Additionally, data were corroborated following Haldane relations, where the ratio between the direct/inverse rate constants gives the apparent equilibrium constant ($K_{eq\ app}$) of the catalyzed reaction. For the reaction: 2 GSH + *Tcr*TXN_{Ox} ↔ GSSG + *Tcr*TXN_{Red}, the $K_{eq\ app}$ can be calculated as a relation between a third-order kinetic constant (direct reaction) or a second-order kinetic constant (inverse reaction). Hence, we calculated the $K_{eq\ app}$ for the reaction and, utilizing the Nernst equation, we obtained the global standard redox potential at pH 7.5 for each *Tcr*TXN. Values for *Tcr*TXNI and *Tcr*TXNIIΔ22C were calculated in -232 ± 5 mV and -214 ± 9 mV, respectively (similar to those values obtained by the equilibrium method with the GSSG/GSH couple).

Measurement of the thiol ionization states of T. cruzi TXNs at 240 nm

Determination of thiolate states were performed monitoring the absorption spectrum of reduced and oxidized *Tcr*TXNI and *Tcr*TXNIIΔ22C between 200 and 340 nm in a pH range from 5 to 10 (data no shown). The thiolate anion has a significant absorption at 240 nm, whereas the thiol form does not [10, 40]. Spectra of the respective reduced and oxidized TXNs overlapped, except for the region between 240 nm and 270 nm where the absorption of reduced TXNs was raised with increasing pH. Changes in ε values at 240 nm reflect ionization of the thiols, at 295 nm tyrosine ionization and at 288 nm unfolding of the protein [10, 39, 40]. Subtracting ε_{240} values for oxidized and reduced TXNs, resulted in a titration curve with two inflection points (Figure 6), from where p*Ka* values were derived after fitting data with the Henderson-Hasselbalch equation [40]. Thus, pKa_1 of 7.0 ± 0.1 and pKa_2 of 9.3 ± 0.4 for *Tcr*TXNI and pKa_1 of 7.3 ± 0.2 and pKa_2 of 9.0 ± 0.3 for *Tcr*TXNIIΔ22C were calculated (Figure 6). Values of p*Ka* were consistent with inflection points observed from pH-profile activity for *Tcr*TXNs (Figure 6 – inset), indicating the strong dependence of the ionization state of redox active cysteines for disulfide reductase

activity of these proteins. In addition, the pKa_1 value that probably is related to the nucleophilic cysteine of *Tcr*TXNs (Cys^{40} in both proteins) is similar to that reported for *T. brucei* TXNI [10].

Redox titration of T. cruzi thiol-dependent peroxidases

Redox titrations were realized by incubation of proteins with different molar ratios of reduced and oxidized glutathione or 2-mercaptoethanol, followed by analysis by non-reducing SDS-PAGE and densitometry (Supplemental data – Figure 4). Using this methodology we determined the midpoint global redox potential at pH 7.5 and 30 ºC ($E_{m7.5}$) of -196 ± 3 mV for *Tcr*cTXNPx, -142 ± 4 mV for *Tcr*mTXNPx and -96 ± 6 mV for *Tcr*GPxI (Supplemental data – Figure 5). Similar results were obtained with both redox couple buffers (glutathione or 2-mercaptoethanol). Redox potentials for the thiol-dependent peroxidases analyzed are physiologically coherent in or with respect to those exhibited by their reducing substrates, *Tcr*TXNs (average value of -230 mV, see above). In addition, these values are in the range of those reported for other members of the thiol-dependent peroxidases family (for example, AhpC from *Salmonella typhimurium* of -178 mV [48]).

Expression and subcellular localization of TcrTXNII

The expression of *Tcr*TXNII in various stages of *T. cruzi* was evaluated in a western blot assay using polyclonal anti-*Tcr*TXNII serum and total extracts from *T. cruzi* forms. As shown in Figure 7-A, positive signals were detected in extracts from three stages of the parasite (epimastigote, trypomastigote and amastigote). In addition, the images obtained by indirect immunofluorescence microscopy in epimastigote, trypomastigote and amastigote cells (Figure 7-B) revealed a pattern of recognition signals compatible with a vesicular distribution. To confirm that *Tcr*TXNII is an integral membrane protein, we performed an extraction of total membrane proteins with alkaline carbonate on insoluble fraction of epimastigote cells (total membranes). Figure 8 shows that *Tcr*TXNII was recovered in the insoluble fractions of parasite lysates and not solubilized with alkaline carbonate buffer. In addition, *Tcr*TXNII was also detected in the insoluble fraction obtained after treatment of supernatant-lysate with $CaCl_2$, suggesting that the protein could also occur in vesicles and/or microsomes. This result correlates with the

observed vesicular pattern in the indirect immunofluorescence microscopy in epimastigotes. *Tcr*TXNI was detected only in the soluble fractions, indicating that it is a soluble protein that does not interact with membranes.

Subcellular localization and topology of *Tcr*TXNII was further analyzed by digitonin extraction and proteinase K protection assays of *T. cruzi* epimastigotes. Our results suggest a location of *Tcr*TXNII at the endo-membrane systems like glycosome, mitochondrial outer membrane and/or endoplasmatic reticulum (Figure 9) with its redox-active domain exposed to the cytosol (see Figure 10). A plasmatic membrane location was discarded. As shown in Figure 10, the protein was digested at digitonin concentrations that expose cytosolic proteins (*Tcr*cTXNPx) and but not endoplasmatic (*Tcr*BIP or *Tcr*APx) or mitochondrial intermembrane space (*Tcr*CytC) proteins. Similar results were previously reported for *Leishmania infantum* TXNIII, which exhibited an external mitochondrial membrane localization [22].

DISCUSSION

Once inoculated into a mammalian host, *T. cruzi* depends on its capacity to infect cells and, within these cells, differentiate and replicate [49]. To succeed in this complex sequence of events, parasites must be equipped to deal with toxic oxidants, such as reactive oxygen and nitrogen species (ROS and RNS, respectively), generated as consequence of their own aerobic metabolism and as part of the host's antimicrobial defense [49]. The pathogen ability to resist oxidative stress is essential for survival during infection of mammalian tissues [1, 50]. Currently, there is a general understanding about the mechanisms responsible for this resistance, but characterization of the various components in redox metabolism is far from being completed. In trypanosomatids, TXNs transfer reducing equivalents from trypanothione to redox pathways involving thiol/disulfide exchange [4, 9]. Several TXN-dependent enzymes have also been identified within several intracellular compartments, for example, into the mitochondrion, implying that an active TXN should also be present within these subcellular compartments [2, 49, 50]. Herein, we analyze the expression and functional characterization of a second TXN from *T. cruzi* (*Tcr*TXNII) that can be described as an additional component in the ROS and RNS detoxification pathways of the parasite. Figure 11 details the many pathways where TXNs are involved in

trypanosomatids metabolism. To the best of our knowledge, this is the first detailed study of this type protein from *T. cruzi*.

Herein we revisited the redox metabolism related to TXNs in *T. cruzi*, pointing out that *Tcr*TXNII could be itself a functional TXN of relevance for the parasite redox metabolism. Previous phylogenetic analysis [22] revealed that *Tcr*TXNII could belong to class II of TXNs (together with *L. infantum* TXNIII and *T. brucei* TXNII), distinct from class I, which contains the TXNI of all trypanosomatids and the TXNII sequence of *Leishmania* and *Crithidia* [11, 21]. Contrary to its characterized *Leishmania* orthologous [22] (*L. infantum* TXNIII), *Tcr*TXNII exhibited TXN activity, being able to transfer reducing equivalents [at expense of $T(SH)_2$] not only to *T. cruzi* cytoplasmatic (*Tcr*cTXNPx), mitochondrial (*Tcr*mTXNPx) 2-Cys peroxiredoxins and glutathione peroxidase I (*Tcr*GPxI) but, also to low molecular mass disulfides (such as GSSG and CySSyC) and DHA. Our results support the involvement of *Tcr*TXNII both in hydroperoxide detoxification metabolism and in regeneration of key metabolites. Additionally, we highlight that *Tcr*TXNII might be also a component of the MetSO reduction pathway, being able to reduce both *T. cruzi* MSRA isoforms (Figure 11).

Recombinant *Tcr*TXNIIΔ22C was reduced by GSH, GSP-SH (less efficiently), and dihydrolipoamide (a mitochondrial dithiol). That is a distinctive behavior respect to recombinant *Lin*TXNIII, which showed a slight oxido-reductase activity just in the presence of $T(SH)_2$ [22]. It is clear the existence of a differential enzyme activity between *Tcr*TXNII and *Lin*TXNIII, supported in many structural differences that could justify disparities in their enzymatic behaviors. Thus, *Tcr*TXNII has the same amino acid substitutions found in *Lin*TXNIII when compared to TXNI but conserving the Ser^{40} residue [22]. We point out at this point a 15 amino acids insertion (from His^{84} to His^{100}) present in *Tcr*TXNII, which is absent in *Lin*TXNIII and also, a Lys^{31} (*Tcr*TXNII numeration) highly conserved in *Tcr*TXNII and *Tcr*TXNI, that is replaced by a Glu (basic/acid change) in *Lin*TXNIII. Hence, an in-depth study of different muteins will be necessary to know the nature of the variable enzyme activity. After considering all our results about functionality of *Tcr*TXNII, together with previous experimental works performed on *Tbr*TXNII [51], we are not in agreement with previous conclusions about *Tcr*TXNII functions extrapolated from kinetics analysis performed on *Lin*TXNIII [22].

*Tcr*TXNI and *Tcr*TXNIIΔ22C exhibited similar redox potentials and p*Ka* values of catalytic cysteine, with data comparable to parameters obtained for *T. brucei* TXNI [10]. Thus, the kinetic discrepancies exhibited between *T. cruzi* TXNs are not a consequence of differences in redox capacity or cysteine reactivity of protein active sites. Values of standard redox potential at pH 7.5 determined for trypanosomatid TXNs (average value of −230 mV) thermodynamically justify the capacity of these enzymes to use $T(SH)_2$ [$E^{o\prime}$ of −242 mV [10]], GSH [$E^{o\prime}$ of −240 mV [38]] or dihydrolipoamide [$E^{o\prime}$ of −334 mV [38]] as a reducing substrates. Values of redox potentials determined in this study for *Tcr*TXNs are coherent with a flow of reduction equivalents transported through the trypanothione-dependent system, originally from NADPH ($E^{o\prime}$ of −320 mV [38]), to the final protein thiols, such as, thiol-dependent peroxidases (average $E_{m7.5}$ of −150 mV for TXNPxs and −100 mV for GPxI) or MSRAs [average $E^{o}_{7.5}$ of −181 mV [18]].

We show in this work the first evaluation of TXNs capacity for catalyzing the $T(SH)_2$-dependent reduction of both GSNO and CySNO. Hence, *T. cruzi* TXNs did not exhibit significant differences on second-order kinetic constants for GSNO-reduction; however, *Tcr*TXNIIΔ22C presented two orders of magnitude less than *Tcr*TXNI for CySNO-reduction catalysis. This *Tcr*TXNs *S*-nitrosothiols reduction capacity could be operating as part of an antioxidant system active against the stress generated by ROS. Possibly, GSH (and to a lesser extent free cysteine) would react with NO-derived species, generating GSNO (or CySNO), being regenerated by $T(SH)_2$/*Tcr*TXN system to GSH (or cysteine) and HNO (which at time react with O_2 to generate NO_2^-). Similar mechanisms are proposed for GSNO-reduction in *P. falciparum* and mammalian cells [52, 53]. As schematized in Figure 11, our work support the idea that $T(SH)_2$/*Tcr*TXN system would act as an important mechanism in the regulation of intracellular levels of GSNO (or CySNO) from *T. cruzi* living under conditions of oxidative stress.

We have also established that the TXN/TRX interaction was more efficient in the transference of reduction equivalents than that previously characterized for the $T(SH)_2$/TRX interaction [39]. Here, *Tcr*TXNI could catalyze approximately 10^4 fold the electron transference process from $T(SH)_2$ to *Tcr*TRX in an assay that included insulin as a final electron acceptor [29]. There is a precedent for this type of redoxin-redoxin interaction in trypanosomatids, like that reported for 1Cys-Grx1 reduction by TXNI in *T. brucei* [34].

When bovine insulin was replaced by TXNPxs, no "synergy" was observed, being the reasons for this differential behavior very difficult to analyze due to substrate competitiveness and interactions between *Tcr*TRX, *Tcr*cTXNPx and *Tcr*TXNI. We could find a possible explanation analyzing the previous data on the specific protein-protein interaction between TXN and TXNPx [54], which suggested that the TXN/TXNPx interaction could be stronger than TXN/TRX. Unlike *Tcr*TXNI, *Tcr*TXNIIΔ22C did not exhibit ability to reduce *Tcr*TRX. Probably, the *Tcr*TXNI amino acid residues necessary for interacting with *Tcr*TRX are absent in *Tcr*TXNII. So far, no experimental data exist about this redoxin-redoxin interaction, so these results could be a starting point for further research on the characterization of this type of protein-protein interaction.

The differences found between primary structures of *Tcr*TXNI and *Tcr*TXNII could be responsible for a lower kinetic efficiency of *Tcr*TXNII with respect to *Tcr*TXNI. However, the functionality of *Tcr*TXNII as a true TXN was not affected. When comparing the amino acid sequences of *Tcr*TXNII to class I TXNs, it is possible to identify two major variations: (*i) Tcr*TXNII have in position 74 an Arg residue, where classes I TXNs present a Glu or an Asp. At this point it is important to highlight that an acidic residue in this position was previously described to be important for interaction of TXN with $T(SH)_2$ [55], as well as with TXNPxs [54]. Thus, when the acidic residue was mutated by Arg in both *Cf*TXNII and *Tbr*TXNI, the specific activities of these proteins decreased to 17% and 41% respect to the wild-type [11, 54]; (*ii) Tcr*TXNII has a Arg residue in position 112, instead of a Glu, which is involved in GPx/TXN interaction [56]. These structural changes might explain differences in the kinetic properties characterized for both *Tcr*TXNs.

The identity of *Tcr*TXNII as a true integral membrane protein was confirmed by membrane protein extraction with alkaline carbonate buffer and its expression in *T. cruzi* was determinate by western blot in all three-parasite forms (epimastigote, trypomastigote and amastigote). In addition, immunolocalization, digitonin extraction and proteinase K protection assays let us to exclude the cytoplasmatic membrane as the cellular place for *Tcr*TXNII, which could be associated mainly to a glycosomal, endoplasmatic reticulum and/or outer mitochondrial membrane distribution with a cytoplasmatic orientation of the redox domain. A group of integral membrane proteins, known as tail-anchored protein (TA), is defined by the presence of a soluble N-terminal domain that is anchored to the

phospholipid bilayer by a single segment of hydrophobic amino acids close to the C-terminus. The mode of insertion into membranes of these proteins, many of which play key roles in fundamental intracellular processes, is obligatorily posttranslational, highly specific, and may be subjected to regulatory processes that could modulate the protein's function. *Tcr*TXNII belongs to this protein group, recognized as critical for the normal functioning of different organelles [57]. *In vitro* oxido-reductase activity of *Tcr*TXNII suggests that it is involved in redox-dependent biological processes, similar to those described for TRX-like proteins [58], which are macromolecules that can be involved in several cellular pathways like antioxidant defense [58-60], chaperone function [61], cytochrome c assembly [62], and intracellular redox signaling [58, 63, 64]. Previous reports have described the features that determine specific targeting of tail-anchored proteins to the mitochondrial outer membrane or endoplasmatic reticulum [65, 66]. A short transmembrane domain, flanked on both sides by positively charged residues, determines targeting to the mitochondrial outer membrane. Loss of either of these features results in targeting to the endoplasmatic reticulum. Proteins bearing tails with intermediate features, i.e., a slightly lengthened hydrophobic domain and/or reduced positive charge, may be delivered to both the mitochondrial outer membrane and the endoplasmatic reticulum [57]. Targeting and insertion are in some cases subject to regulation by cellular targeting machinery. The C-terminal region of *Tcr*TXNII presents intermediate characteristics, which suggest a dual localization of this protein (both in mitochondrial outer membrane as endoplasmatic reticulum). This observation is consistent with our results obtained after digitonin subcellular fractionation and immunodetection.

Our data support *Tcr*TXNII as a new metabolic component that could act as an important tool not only for the antioxidant response but also in the regulation of other metabolic routes (Figure 11). We feel tempted to speculate that *Tcr*TXNII would function as a suitable complement to other TXNs useful to maintain redox homeostasis within the parasite. The overall results encourages us to continue the in depth characterization of the many cellular partners of TXNII, as well as to perform reverse genetic studies, in order to fully explore their physiological roles to reach a complete scenario of the redox metabolism in trypanosomatids.

REFERENCES

[1] Irigoin, F.; Cibils, L.; Comini, M. A.; Wilkinson, S. R.; Flohé, L.; Radi, R. Insights into the redox biology of Trypanosoma cruzi: Trypanothione metabolism and oxidant detoxification. *Free Radic Biol Med* **45:**733-742; 2008.

[2] Krauth-Siegel, R. L.; Comini, M. A. Redox control in trypanosomatids, parasitic protozoa with trypanothione-based thiol metabolism. *Biochim Biophys Acta* **1780:**1236-1248; 2008.

[3] Pineyro, M. D.; Parodi-Talice, A.; Arcari, T.; Robello, C. Peroxiredoxins from Trypanosoma cruzi: virulence factors and drug targets for treatment of Chagas disease? *Gene* **408:**45-50; 2008.

[4] Gommel, D. U.; Nogoceke, E.; Morr, M.; Kiess, M.; Kalisz, H. M.; Flohé, L. Catalytic characteristics of tryparedoxin. *Eur J Biochem* **248:**913-918; 1997.

[5] Lüdemann, H.; Dormeyer, M.; Sticherling, C.; Stallmann, D.; Follmann, H.; Krauth-Siegel, R. L. Trypanosoma brucei tryparedoxin, a thioredoxin-like protein in African trypanosomes. *FEBS Lett* **431:**381-385; 1998.

[6] Kalisz, H. M.; Hofmann, B.; Nogoceke, E.; Gommel, D. U.; Flohé, L.; Hecht, H. J. Crystallisation of tryparedoxin I from Crithidia fasciculata. *Biofactors* **11:**73-75; 2000.

[7] Guerrero, S. A.; Montemartini, M.; Spallek, R.; Hecht, H. J.; Steinert, P.; Flohé, L.; Singh, M. Cloning and expression of tryparedoxin I from Crithidia fasciculata. *Biofactors* **11:**67-69; 2000.

[8] Montemartini, M.; Nogoceke, E.; Gommel, D. U.; Singh, M.; Kalisz, H. M.; Steinert, P.; Flohé, L. Tryparedoxin and tryparedoxin peroxidase. *Biofactors* **11:**71-72; 2000.

[9] Flohé, L.; Steinert, P.; Hecht, H. J.; Hofmann, B. Tryparedoxin and tryparedoxin peroxidase. *Methods Enzymol* **347:**244-258; 2002.

[10] Reckenfelderbaumer, N.; Krauth-Siegel, R. L. Catalytic properties, thiol pK value, and redox potential of Trypanosoma brucei tryparedoxin. *J Biol Chem* **277:**17548-17555; 2002.

[11] Steinert, P.; Plank-Schumacher, K.; Montemartini, M.; Hecht, H. J.; Flohé, L. Permutation of the active site motif of tryparedoxin 2. *Biol Chem* **381:**211-219; 2000.

[12] Castro, H.; Romao, S.; Gadelha, F. R.; Tomas, A. M. Leishmania infantum: provision of reducing equivalents to the mitochondrial tryparedoxin/tryparedoxin peroxidase system. *Exp Parasitol* **120:**421-423; 2008.

[13] Trujillo, M.; Ferrer-Sueta, G.; Thomson, L.; Flohé, L.; Radi, R. Kinetics of peroxiredoxins and their role in the decomposition of peroxynitrite. *Subcell Biochem* **44:**83-113; 2007.

[14] Schlecker, T.; Schmidt, A.; Dirdjaja, N.; Voncken, F.; Clayton, C.; Krauth-Siegel, R. L. Substrate specificity, localization, and essential role of the glutathione peroxidase-type tryparedoxin peroxidases in Trypanosoma brucei. *J Biol Chem* **280:**14385-14394; 2005.

[15] Trujillo, M.; Budde, H.; Pineyro, M. D.; Stehr, M.; Robello, C.; Flohé, L.; Radi, R. Trypanosoma brucei and Trypanosoma cruzi tryparedoxin peroxidases catalytically detoxify peroxynitrite via oxidation of fast reacting thiols. *J Biol Chem* **279:**34175-34182; 2004.

[16] Krauth-Siegel, R. L.; Schmidt, H. Trypanothione and tryparedoxin in ribonucleotide reduction. *Methods Enzymol* **347:**259-266; 2002.

[17] Wilkinson, S. R.; Meyer, D. J.; Taylor, M. C.; Bromley, E. V.; Miles, M. A.; Kelly, J. M. The Trypanosoma cruzi enzyme TcGPXI is a glycosomal peroxidase and can be linked to trypanothione reduction by glutathione or tryparedoxin. *J Biol Chem* **277:**17062-17071; 2002.

[18] Arias, D. G.; Cabeza, M. S.; Erben, E. D.; Carranza, P. G.; Lujan, H. D.; Tellez Inon, M. T.; Iglesias, A. A.; Guerrero, S. A. Functional characterization of methionine sulfoxide reductase A from Trypanosoma spp. *Free Radic Biol Med* **50:**37-46; 2011.

[19] Comini, M. A.; Krauth-Siegel, R. L.; Flohé, L. Depletion of the thioredoxin homologue tryparedoxin impairs antioxidative defence in African trypanosomes. *Biochem J* **402:**43-49; 2007.

[20] Romao, S.; Castro, H.; Sousa, C.; Carvalho, S.; Tomas, A. M. The cytosolic tryparedoxin of Leishmania infantum is essential for parasite survival. *Int J Parasitol* **39:**703-711; 2009.

[21] Castro, H.; Sousa, C.; Novais, M.; Santos, M.; Budde, H.; Cordeiro-da-Silva, A.; Flohé, L.; Tomas, A. M. Two linked genes of Leishmania infantum encode tryparedoxins localised to cytosol and mitochondrion. *Mol Biochem Parasitol* **136:**137-147; 2004.

[22] Castro, H.; Romao, S.; Carvalho, S.; Teixeira, F.; Sousa, C.; Tomas, A. M. Mitochondrial redox metabolism in trypanosomatids is independent of tryparedoxin activity. *PLoS One* **5:**e12607; 2010.

[23] El-Sayed, N. M.; Myler, P. J.; Bartholomeu, D. C.; Nilsson, D.; Aggarwal, G.; Tran, A. N.; Ghedin, E.; Worthey, E. A.; Delcher, A. L.; Blandin, G.; Westenberger, S. J.; Caler, E.; Cerqueira, G. C.; Branche, C.; Haas, B.; Anupama, A.; Arner, E.; Aslund, L.; Attipoe, P.; Bontempi, E.; Bringaud, F.; Burton, P.; Cadag, E.; Campbell, D. A.; Carrington, M.; Crabtree, J.; Darban, H.; da Silveira, J. F.; de Jong, P.; Edwards, K.; Englund, P. T.; Fazelina, G.; Feldblyum, T.; Ferella, M.; Frasch, A. C.; Gull, K.; Horn, D.; Hou, L.; Huang, Y.; Kindlund, E.; Klingbeil, M.; Kluge, S.; Koo, H.; Lacerda, D.; Levin, M. J.; Lorenzi, H.; Louie, T.; Machado, C. R.; McCulloch, R.; McKenna, A.; Mizuno, Y.; Mottram, J. C.; Nelson, S.; Ochaya, S.; Osoegawa, K.; Pai, G.; Parsons, M.; Pentony, M.; Pettersson, U.; Pop, M.; Ramirez, J. L.; Rinta, J.; Robertson, L.; Salzberg, S. L.; Sanchez, D. O.; Seyler, A.; Sharma, R.; Shetty, J.; Simpson, A. J.; Sisk, E.; Tammi, M. T.; Tarleton, R.; Teixeira, S.; Van Aken, S.; Vogt, C.; Ward, P. N.; Wickstead, B.; Wortman, J.; White, O.; Fraser, C. M.; Stuart, K. D.; Andersson, B. The genome sequence of Trypanosoma cruzi, etiologic agent of Chagas disease. *Science* **309:**409-415; 2005.

[24] Gomez, M. L.; Erijman, L.; Arauzo, S.; Torres, H. N.; Tellez-Inon, M. T. Protein kinase C in Trypanosoma cruzi epimastigote forms: partial purification and characterization. *Mol Biochem Parasitol* **36:**101-108; 1989.

[25] Allaoui, A.; Francois, C.; Zemzoumi, K.; Guilvard, E.; Ouaissi, A. Intracellular growth and metacyclogenesis defects in Trypanosoma cruzi carrying a targeted deletion of a Tc52 protein-encoding allele. *Mol Microbiol* **32:**1273-1286; 1999.

[26] Andrews, N. W.; Colli, W. Adhesion and interiorization of Trypanosoma cruzi in mammalian cells. *J Protozool* **29:**264-269; 1982.

[27] Maniatis, T.; Fritsch, E. F.; Sambrook, J. *Molecular Cloning: A laboratory Manual.* N. Y. - USA: Cold Spring Harhor; 1982.

[28] Sullivan, F. X.; Walsh, C. T. Cloning, sequencing, overproduction and purification of trypanothione reductase from Trypanosoma cruzi. *Mol Biochem Parasitol* **44:**145-147; 1991.

[29] Piattoni, C. V.; Blancato, V. S.; Miglietta, H.; Iglesias, A. A.; Guerrero, S. A. On the occurrence of thioredoxin in Trypanosoma cruzi. *Acta Trop* **97:**151-160; 2006.
[30] Guerrero, S. A.; Lopez, J. A.; Steinert, P.; Montemartini, M.; Kalisz, H. M.; Colli, W.; Singh, M.; Alves, M. J.; Flohé, L. His-tagged tryparedoxin peroxidase of Trypanosoma cruzi as a tool for drug screening. *Appl Microbiol Biotechnol* **53:**410-414; 2000.
[31] Laemmli, U. K. Cleavage of structural proteins during the assembly of the head of bacteriophage T4. *Nature* **227:**680-685; 1970.
[32] Bradford, M. M. A rapid and sensitive method for the quantitation of microgram quantities of protein utilizing the principle of protein-dye binding. *Anal Biochem* **72:**248-254; 1976.
[33] Vaitukaitis, J.; Robbins, J. B.; Nieschlag, E.; Ross, G. T. A method for producing specific antisera with small doses of immunogen. *J Clin Endocrinol Metab* **33:**988-991; 1971.
[34] Filser, M.; Comini, M. A.; Molina-Navarro, M. M.; Dirdjaja, N.; Herrero, E.; Krauth-Siegel, R. L. Cloning, functional analysis, and mitochondrial localization of Trypanosoma brucei monothiol glutaredoxin-1. *Biol Chem* **389:**21-32; 2008.
[35] Flohe, L.; Steinert, P.; Hecht, H. J.; Hofmann, B. Tryparedoxin and tryparedoxin peroxidase. *Methods Enzymol* **347:**244-258; 2002.
[36] Sedlak, J.; Lindsay, R. H. Estimation of total, protein-bound, and nonprotein sulfhydryl groups in tissue with Ellman's reagent. *Anal Biochem* **25:**192-205; 1968.
[37] Forman, H.; Fukuto, J.; Torres, M. *Signal Transduction by Reactive Oxygen and Nitrogen Species: Pathways and Chemical Principles.* Kluwer Academic Publisher; 2004.
[38] Schafer, F. Q.; Buettner, G. R. Redox environment of the cell as viewed through the redox state of the glutathione disulfide/glutathione couple. *Free Radic Biol Med* **30:**1191-1212; 2001.
[39] Schmidt, H.; Krauth-Siegel, R. L. Functional and physicochemical characterization of the thioredoxin system in Trypanosoma brucei. *J Biol Chem* **278:**46329-46336; 2003.
[40] Nelson, J. W.; Creighton, T. E. Reactivity and ionization of the active site cysteine residues of DsbA, a protein required for disulfide bond formation in vivo. *Biochemistry* **33:**5974-5983; 1994.
[41] Schenkman, J. B.; Cinti, D. L. Preparation of microsomes with calcium. *Methods Enzymol* **52:**83-89; 1978.
[42] Ceylan, S.; Seidel, V.; Ziebart, N.; Berndt, C.; Dirdjaja, N.; Krauth-Siegel, R. L. The dithiol glutaredoxins of african trypanosomes have distinct roles and are closely linked to the unique trypanothione metabolism. *J Biol Chem* **285:**35224-35237; 2010.
[43] Xiao, R.; Lundstrom-Ljung, J.; Holmgren, A.; Gilbert, H. F. Catalysis of thiol/disulfide exchange. Glutaredoxin 1 and protein-disulfide isomerase use different mechanisms to enhance oxidase and reductase activities. *J Biol Chem* **280:**21099-21106; 2005.
[44] Gilbert, H. F. Catalysis of thiol/disulfide exchange: single-turnover reduction of protein disulfide-isomerase by glutathione and catalysis of peptide disulfide reduction. *Biochemistry* **28:**7298-7305; 1989.
[45] Krauth-Siegel, R. L.; Lüdemann, H. Reduction of dehydroascorbate by trypanothione. *Mol Biochem Parasitol* **80:**203-208; 1996.
[46] Aslund, F.; Berndt, K. D.; Holmgren, A. Redox potentials of glutaredoxins and other thiol-disulfide oxidoreductases of the thioredoxin superfamily determined by direct protein-protein redox equilibria. *J Biol Chem* **272:**30780-30786; 1997.

[47] Pineyro, M. D.; Parodi-Talice, A.; Portela, M.; Arias, D. G.; Guerrero, S. A.; Robello, C. Molecular characterization and interactome analysis of Trypanosoma cruzi tryparedoxin 1. *J Proteomics* **74:**1683-1692.
[48] Parsonage, D.; Karplus, P. A.; Poole, L. B. Substrate specificity and redox potential of AhpC, a bacterial peroxiredoxin. *Proc Natl Acad Sci U S A* **105:**8209-8214; 2008.
[49] Piacenza, L.; Alvarez, M. N.; Peluffo, G.; Radi, R. Fighting the oxidative assault: the Trypanosoma cruzi journey to infection. *Curr Opin Microbiol* **12:**415-421; 2009.
[50] Alvarez, M. N.; Peluffo, G.; Piacenza, L.; Radi, R. Intraphagosomal peroxynitrite as a macrophage-derived cytotoxin against internalized Trypanosoma cruzi: Consequences for oxidative killing and role of microbial peroxiredoxins in infectivity. *J Biol Chem* **268:**6627-6640; 2011.
[51] Motyka, S. A.; Drew, M. E.; Yildirir, G.; Englund, P. T. Overexpression of a cytochrome b5 reductase-like protein causes kinetoplast DNA loss in Trypanosoma brucei. *J Biol Chem* **281:**18499-18506; 2006.
[52] Kanzok, S. M.; Rahlfs, S.; Becker, K.; Schirmer, R. H. Thioredoxin, thioredoxin reductase, and thioredoxin peroxidase of malaria parasite Plasmodium falciparum. *Methods Enzymol* **347:**370-381; 2002.
[53] Nikitovic, D.; Holmgren, A. S-nitrosoglutathione is cleaved by the thioredoxin system with liberation of glutathione and redox regulating nitric oxide. *J Biol Chem* **271:**19180-19185; 1996.
[54] Budde, H.; Flohé, L.; Hecht, H. J.; Hofmann, B.; Stehr, M.; Wissing, J.; Lünsdorf, H. Kinetics and redox-sensitive oligomerisation reveal negative subunit cooperativity in tryparedoxin peroxidase of Trypanosoma brucei brucei. *Biol Chem* **384:**619-633; 2003.
[55] Hofmann, B.; Budde, H.; Bruns, K.; Guerrero, S. A.; Kalisz, H. M.; Menge, U.; Montemartini, M.; Nogoceke, E.; Steinert, P.; Wissing, J. B.; Flohé, L.; Hecht, H. J. Structures of tryparedoxins revealing interaction with trypanothione. *Biol Chem* **382:**459-471; 2001.
[56] Melchers, J.; Diechtierow, M.; Feher, K.; Sinning, I.; Tews, I.; Krauth-Siegel, R. L.; Muhle-Goll, C. Structural basis for a distinct catalytic mechanism in Trypanosoma brucei tryparedoxin peroxidase. *J Biol Chem* **283:**30401-30411; 2008.
[57] Mateja, A.; Szlachcic, A.; Downing, M. E.; Dobosz, M.; Mariappan, M.; Hegde, R. S.; Keenan, R. J. The structural basis of tail-anchored membrane protein recognition by Get3. *Nature* **461:**361-366; 2009.
[58] Carvalho, A. P.; Fernandes, P. A.; Ramos, M. J. Similarities and differences in the thioredoxin superfamily. *Prog Biophys Mol Biol* **91:**229-248; 2006.
[59] Fabianek, R. A.; Hennecke, H.; Thony-Meyer, L. Periplasmic protein thiol:disulfide oxidoreductases of Escherichia coli. *FEMS Microbiol Rev* **24:**303-316; 2000.
[60] Brennan, L. A.; Lee, W.; Kantorow, M. TXNL6 is a novel oxidative stress-induced reducing system for methionine sulfoxide reductase a repair of alpha-crystallin and cytochrome C in the eye lens. *PLoS One* **5:**e15421; 2010.
[61] Kim, S. G.; Chi, Y. H.; Lee, J. S.; Schlesinger, S. R.; Zabet-Moghaddam, M.; Chung, J. S.; Knaff, D. B.; Kim, S. T.; Lee, S. Y.; Kim, S. K. Redox properties of a thioredoxin-like Arabidopsis protein, AtTDX. *Biochim Biophys Acta* **1804:**2213-2221; 2010.
[62] Gabilly, S. T.; Dreyfuss, B. W.; Karamoko, M.; Corvest, V.; Kropat, J.; Page, M. D.; Merchant, S. S.; Hamel, P. P. CCS5, a thioredoxin-like protein involved in the assembly of plastid c-type cytochromes. *J Biol Chem* **285:**29738-29749; 2010.

[63] Qu, Y.; Wang, J.; Ray, P. S.; Guo, H.; Huang, J.; Shin-Sim, M.; Bukoye, B. A.; Liu, B.; Lee, A. V.; Lin, X.; Huang, P.; Martens, J. W.; Giuliano, A. E.; Zhang, N.; Cheng, N. H.; Cui, X. Thioredoxin-like 2 regulates human cancer cell growth and metastasis via redox homeostasis and NF-kappaB signaling. *J Clin Invest* **121:**212-225; 2010.
[64] Yoshihara, E.; Chen, Z.; Matsuo, Y.; Masutani, H.; Yodoi, J. Thiol redox transitions by thioredoxin and thioredoxin-binding protein-2 in cell signaling. *Methods Enzymol* **474:**67-82; 2010.
[65] Borgese, N.; Colombo, S.; Pedrazzini, E. The tale of tail-anchored proteins: coming from the cytosol and looking for a membrane. *J Cell Biol* **161:**1013-1019; 2003.
[66] Borgese, N.; Fasana, E. Targeting pathways of C-tail-anchored proteins. *Biochim Biophys Acta* **1808:**937-946.

ACKNOWLEDGMENTS

We thank Dr. James D. Bangs (University of Wisconsin, Madison) for *T. brucei* α-BIP antibody and Dr. Andre Schneider (University of Berne, Switzerland) for *T. brucei* α-cytochrome c antibody. We wish to thank Dr. Shane Wilkinson (School of Biological and Chemical Sciences, Queen Mary University of London) for reading the manuscript and for invaluable suggestions. This work was supported by grants from UNL (CAI+D Orientados & Redes), CONICET (PIP 112 2008-01-02519), and ANPCyT (PICT'07 668 and PICT´08 1754). VEM is fellows from CONICET. DGA, AAI and SAG are investigator career members from CONICET.

FIGURE LEGENDS

Fig. 1: Amino acids sequence alignment of *Tcr*TXNI and *Tcr*TXNII with TXN homologues. *Crithidia fasciculata* TXNI (NCBI Accession Nº AAD20445), *Leishmania infantum* TXNI (TriTrypDB Accession Nº LinJ29_V3.1250), *Crithidia fasciculata* TXNII (NCBI Accession Nº AAC61984), *Leishmania infantum* TXNII (TriTrypDB Accession Nº LinJ29_V3.1240), *Trypanosoma brucei* TXNI (TriTrypDB Accession Nº Tb927.3.3780), *Leishmania infantum* TXNIII (TriTrypDB Accession Nº LinJ31_V3.2000), *Trypanosoma brucei* TXNII (TriTrypDB Accession Nº Tb927.3.5090). Each individual sequence is numbered accordingly. The arrows show the redox active motif.

Fig. 2: Trypanothione-dependent disulfide reductase activity of *T. cruzi* redoxins. The reactions were performed at 30 ºC in 100 mM Tris–HCl, pH 7.5, 2 mM EDTA, 300 μM NADPH, 1 μM *Tcr*TR, 100 μM TS_2, 100 μM bovine insulin and with either different concentrations of *Tcr*TXNI (■), *Tcr*TXNIIΔ22C (○), or *Tcr*TRX (▲).

Fig. 3: A) Kinetic analysis of *T. cruzi* Prxs and GPx reduction by *Tcr*TXNIIΔ22C. The reactions were performed in 100 mM Tris–HCl, pH 7.5, 2 mM EDTA, 300 μM NADPH, 1 μM *Tcr*TR, 100 μM TS_2, different concentrations of *Tcr*TXNIIΔ22C, 70 μM *t*-bOOH and 0.26 μM *Tcr*cTXNPx (■) or 1.2 μM *Tcr*GPxI (○) or 1 μM *Tcr*mTXNPx (▲), at 30 ºC. **B) Kinetic analysis of *T. cruzi* MSRAs reduction by *Tcr*TXNIIΔ22C.** The reactions were performed in 100 mM Tris–HCl, pH 7.5, 2 mM EDTA, 300 μM NADPH, 1 μM *Tcr*TR, 100 μM TS_2, different concentrations of *Tcr*TXNIIΔ22C, 2.5 mM L-Met(*S*)SO and 4 μM *Tcr*MSRA10 (■) or 10 μM *Tcr*MSRA180 (○), at 30 ºC.

Fig. 4: Reduction of *Tcr*TXNs by GSH. The reactions were performed in 100 mM Tris–HCl, pH 7.5, 2 mM EDTA, 200 μM NADPH, 1 $U \cdot ml^{-1}$ GR, 5 μM *Tcr*cTXNPx, 70 μM *t*-bOOH, 0.5-2 μM *Tcr*TXNI (■) or *Tcr*TXNIIΔ22C (○), and different concentration of GSH at 30 ºC.

Fig. 5: Kinetic of *Tcr*TRX reduction by *Tcr*TXNI. The reactions were performed in 100 mM Tris–HCl, pH 7.5, 2 mM EDTA, 300 μM NADPH, 1 μM *Tcr*TR, 100 μM TS_2, 100 μM bovine insulin and different concentration of *Tcr*TRX at different concentrations of *Tcr*TXNI: 0 μM (■), 0.25 μM (○), 0.5 μM (🖷) and 1 μM (▽), at 30 ºC.

Fig. 6: *T. cruzi* TXNs cysteine thiolate titration by 240 nm absorption. Thiolate titrations of *Tcr*TXNI (■) and *Tcr*TXNIIΔ22C (○) were carried out with 10 μM of each TXN in 100 mM of buffer solution (see materials and methods) at 25 °C. Inset: pH-dependent profile for GSSG reductase activity of *T. cruzi* TXNs, at 30 ºC.

Fig. 7: Expression of *Tcr*TXNII during the life cycle of *T. cruzi.* A) Western blot using 40 μg of *T. cruzi* crude extract from epimastigotes (Epi), trypomastigotes (Try) and amastigotes (Ama). B) **Confocal microscopy images of intracellular amastigotes (I), trypomastigotes (II) or epimastigotes (III) expressing *Tcr*TXNII.** Parasites were stained with TOPRO-3 for visualization of nucleus and kinetoplast (blue) and labeled with anti-*Tcr*TXNII antibody and Alexa488 conjugated goat anti-IgG as a secondary antibody (green).

Fig. 8: Extraction of vesicular and membrane proteins. *T. cruzi* epimastigotes were suspended in 10 mM Tris-HCl pH 7.5, 1 mM EDTA and disrupted by sonication and then the lysate centrifuged. The soluble and insoluble fractions were treated with 8 mM $CaCl_2$ and 0.1 M Na_2CO_3 pH 11.0, respectively. After incubation, the samples were centrifuged and soluble and insoluble fractions obtained in both procedures were analyzed by western blot using specific polyclonal sera against *Tcr*TXNII or *Tcr*TXNI (as control for soluble protein).

Fig. 9: Digitonin titration *of Tcr*TXNII in *T. cruzi* epimastigotes. Epimastigote cells were treated with increasing digitonin concentrations. The supernatants were analyzed by western blot using specific polyclonal antibodies against different cellular targets: *Tcr*TXNII (diluted 1/1000), *Tcr*cTXNPx (diluted 1/1000), *Tcr*mXNPx (diluted 1/1000), *Tae*GAPDH (diluted 1/500), *Tcr*BIP (diluted 1/1000) and *Tcr*CytC (diluted 1/500). TRIPC-conjugated goat anti-rabbit (diluted 1/10000) was used as secondary antibody.

Fig. 10: Digitonin extraction and proteinase K protection assay. *T. cruzi* epimastigotes were permeabilized with increasing digitonin concentrations in the presence of proteinase K. The samples were analyzed by western blot using specific polyclonal antibodies against *Tcr*TXNII, *Tcr*cTXNPx (cytosolic protein), *Tcr*BIP and *Tcr*APx (endoplasmatic proteins) and *Tcr*CytC (mitochondrial intermembrane space protein).

Fig. 11: Schematic representation of redox scenario associated to tryparedoxins in trypanosomatids.

Table 1: Kinetic parameters for *T. cruzi* Prxs, GPx and MSRAs reduction by *Tcr*TXNs, calculated in presence of 100 μM $T(SH)_2$ at pH 7.5 and 30 ºC.

Enzyme	Cosubstrate	Parameter	TXN substrate	
			***Tcr*TXNI**	***Tcr*TXNIIΔ22C**
***Tcr*cTXNPx**	*t*-bOOH 70 μM	$k_{cat\ app}$ (s^{-1})	2.016	0.550
		Km_{app} (μM)	6.8	4.7
		$k_{cat\ app}{\cdot}Km_{app}^{-1}$ ($M^{-1}{\cdot}s^{-1}$)	$3.0\cdot 10^5$	$1.2{\cdot}10^5$
***Tcr*mTXNPx**		$k_{cat\ app}$ (s^{-1})	1.833	0.072
		Km_{app} (μM)	16	4.5
		$k_{cat\ app}{\cdot}Km_{app}^{-1}$ ($M^{-1}{\cdot}s^{-1}$)	$1.1\cdot 10^5$	$1.6{\cdot}10^4$
***Tcr*GPxI**		$k_{cat\ app}$ (s^{-1})	0.517	0.158
		Km_{app} (μM)	1.0	11
		$k_{cat\ app}{\cdot}Km_{app}^{-1}$ ($M^{-1}{\cdot}s^{-1}$)	$5.1{\cdot}10^5$	$1.4{\cdot}10^4$
***Tcr*MSRA10**	L-Met(*S*)SO 2.5 mM	$k_{cat\ app}$ (s^{-1})	0.417	0.028
		Km_{app} (μM)	33	16
		$k_{cat\ app}{\cdot}Km_{app}^{-1}$ ($M^{-1}{\cdot}s^{-1}$)	$1.2{\cdot}10^4$	$1.7{\cdot}10^3$
***Tcr*MSRA180**		$k_{cat\ app}$ (s^{-1})	0.028	0.007
		Km_{app} (μM)	0.6	4.6
		$k_{cat\ app}{\cdot}Km_{app}^{-1}$ ($M^{-1}{\cdot}s^{-1}$)	$4.7{\cdot}10^4$	$1.4{\cdot}10^3$

Table 2: Kinetic constants for *T. cruzi* TXN reduction by low molecular mass thiols, calculated in presence of 5 μM *Tcr*cTXNPx and 70 μM *t*-bOOH at pH 7.5 and 30 ºC. N.D.: not determinable.

Reductor	$T(SH)_2$	dihydrolipoamide	GSH		GSP-SH	
	k' ($M^{-1}\cdot s^{-1}$)	k' ($M^{-1}\cdot s^{-1}$)	k' ($M^{-1}\cdot s^{-1}$)	k'' ($M^{-2}\cdot s^{-1}$)	k' ($M^{-1}\cdot s^{-1}$)	k'' ($M^{-2}\cdot s^{-1}$)
***Tcr*TXNI**	$7.3\cdot10^{4}$	$1.1\cdot10^{3}$	62	$2.7\cdot10^{5}$	$2.6\cdot10^{2}$	$2.3\cdot10^{7}$
***Tcr*TXNIIΔ22C**	$2.4\cdot10^{3}$	$3.8\cdot10^{2}$	20	$2.1\cdot10^{5}$	5.1	N.D.

Table 3: Kinetic constants for non-proteins substrates reduction by *T. cruzi* TXNs, calculated in presence of 100 μM $T(SH)_2$ or 3 mM GSH (for DHA reduction) at pH 7.5 and 30 ºC. N.D.: not determinable.

Oxidant	k' ($M^{-1} \cdot s^{-1}$)	
	***Tcr*TXNI**	***Tcr*TXNIIΔ22C**
***Tcr*TRX**	$2.3 \cdot 10^5$	N.D.
GSSG	$1.5 \cdot 10^4$	$2.9 \cdot 10^3$
GSNO	$8.7 \cdot 10^2$	$2.2 \cdot 10^2$
CySNO	$1.4 \cdot 10^2$	1.3
CySSyC	$1.7 \cdot 10^3$	$6.4 \cdot 10^2$
DHA	$1.0 \cdot 10^3$	$5.0 \cdot 10^2$

Highlights

- TXNII is a transmembrane protein with $T(SH)_2$-dependent oxidoreductase activity.
- Reduced TXNII is substrate of methionine sulfoxide reductases and peroxiredoxins.
- TXNI is more efficient than trypanothione in TRX reduction.

Figure1

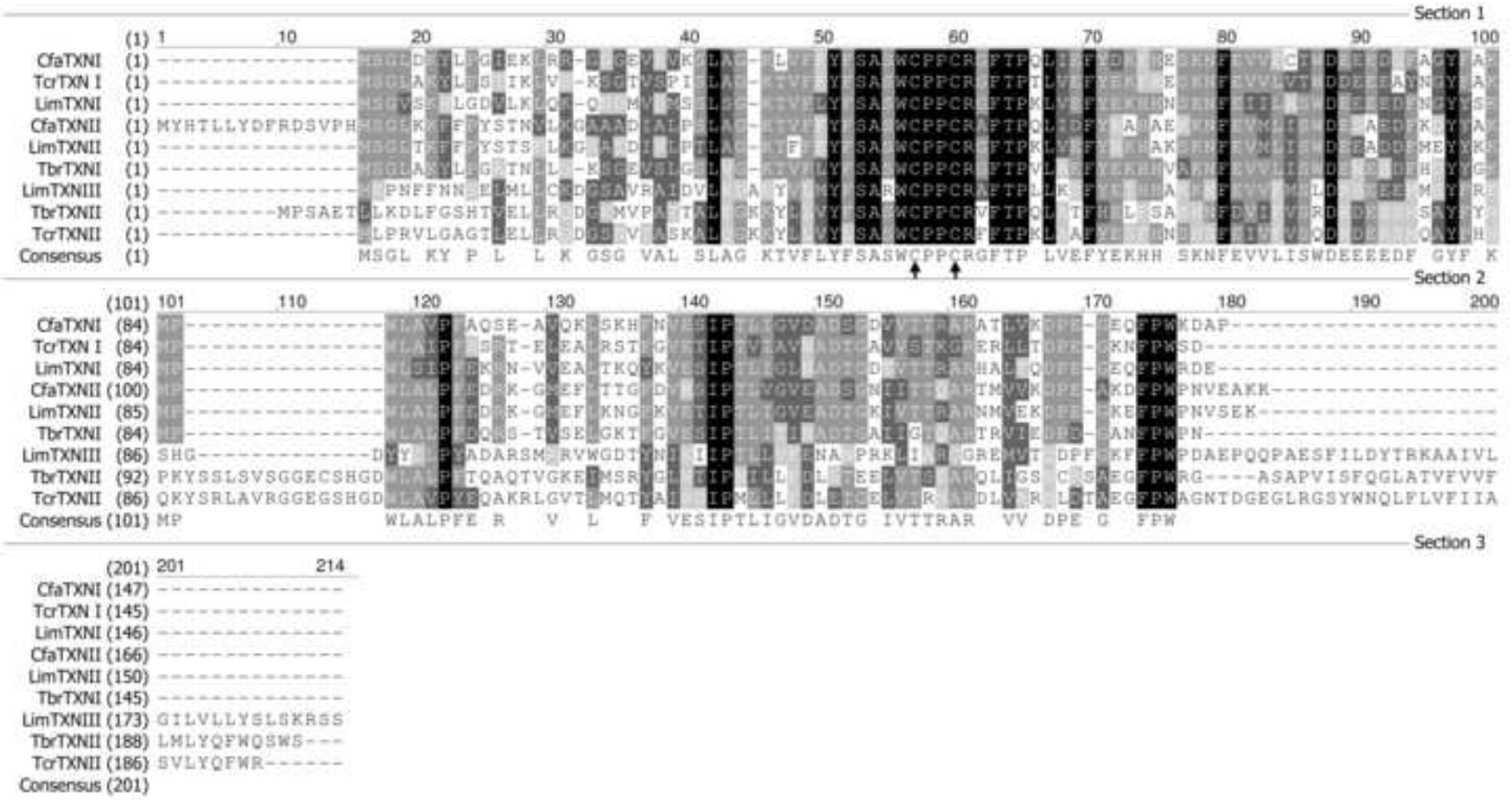

Figure2

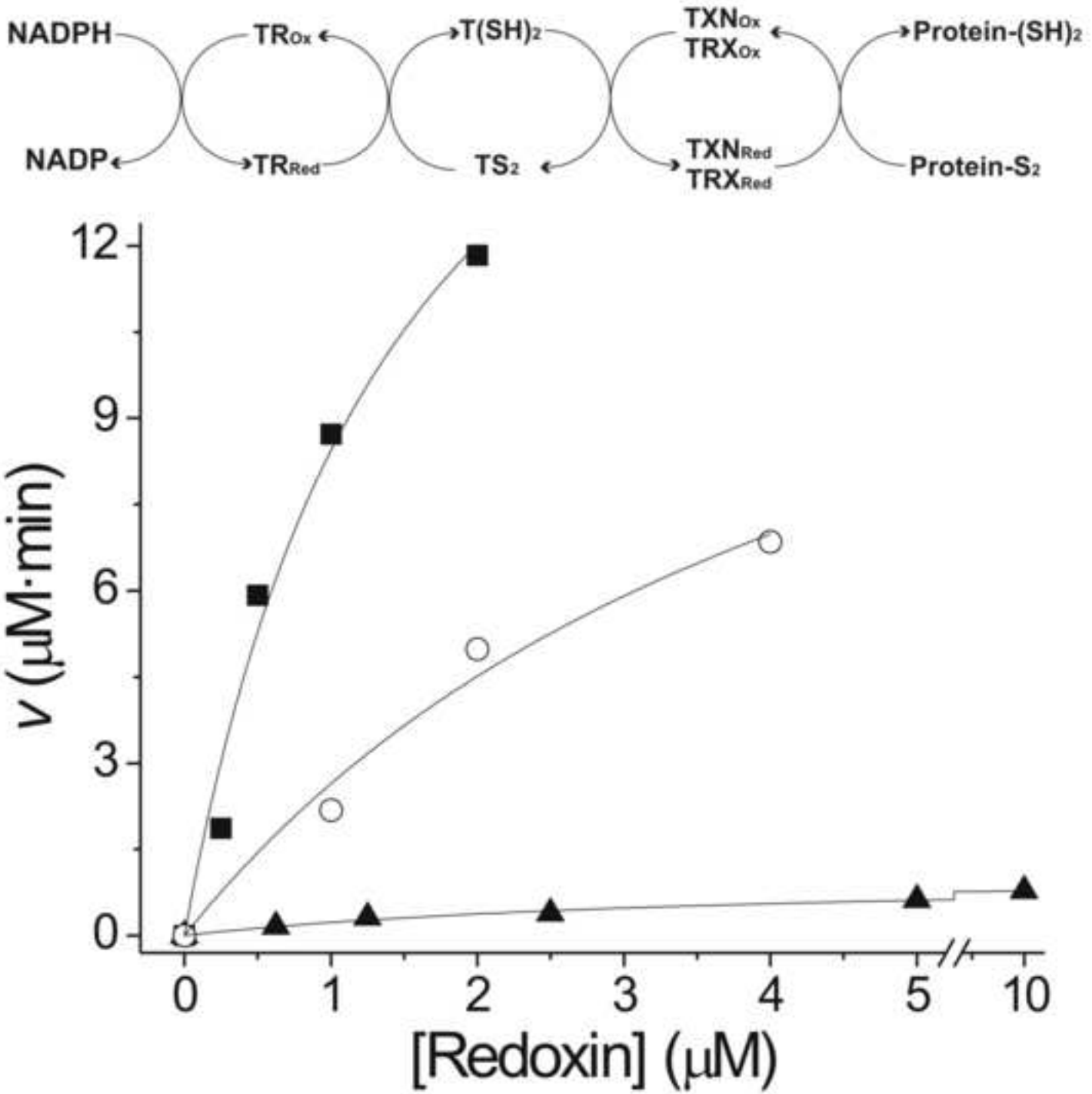

Figure3

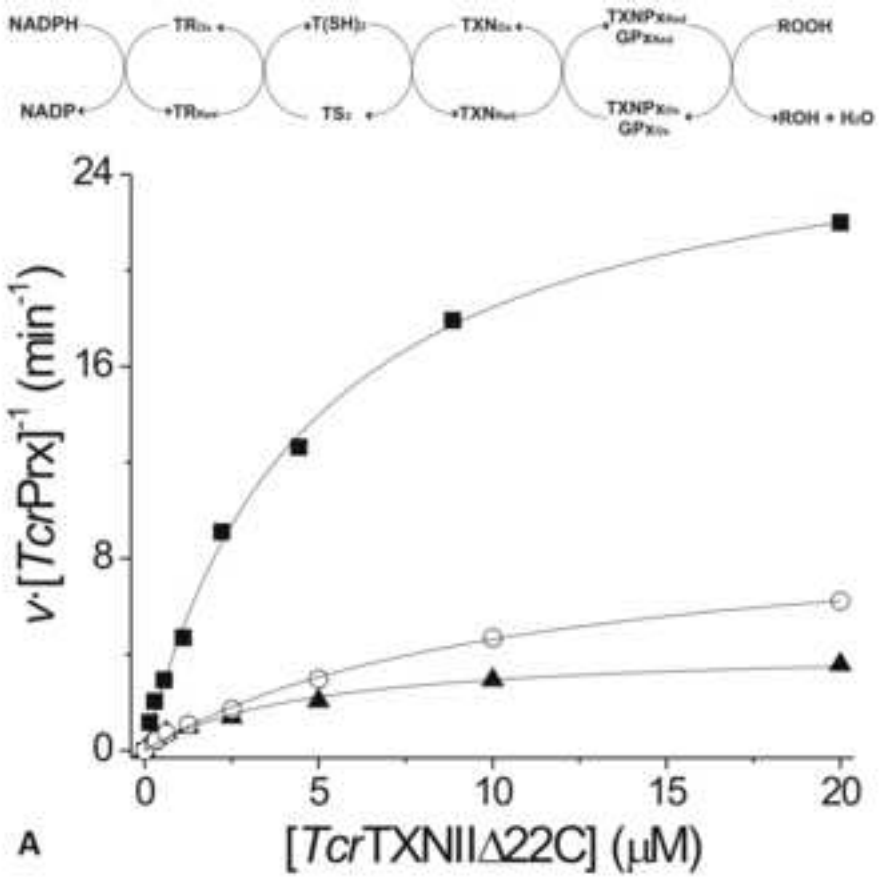

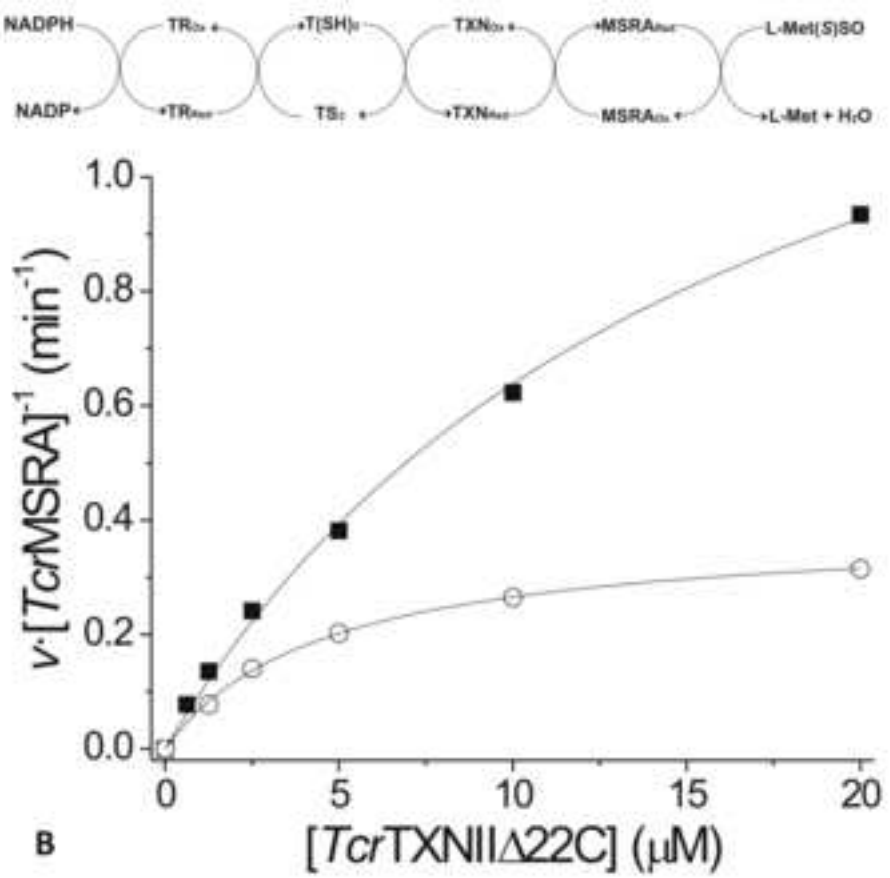

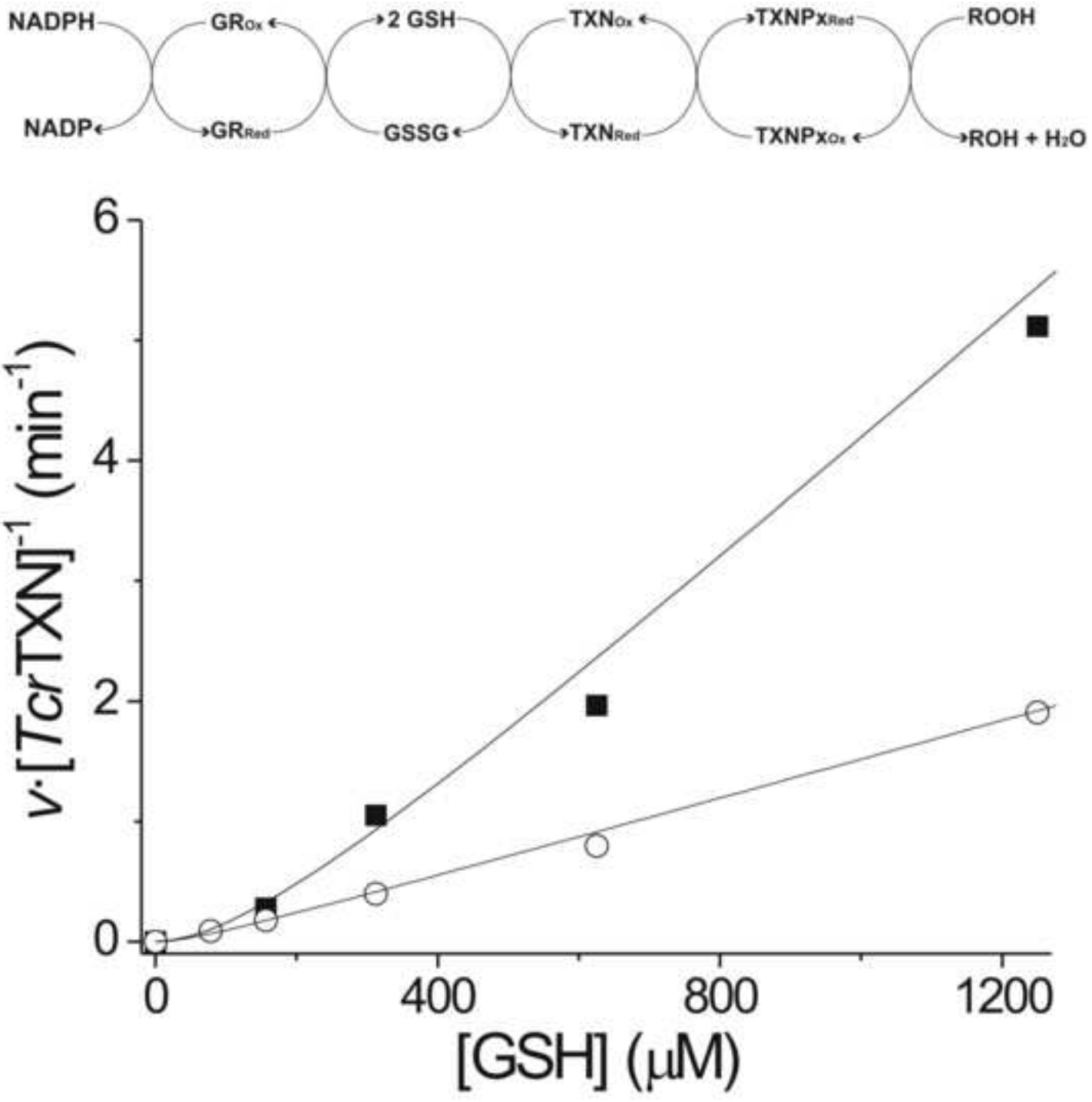

Figure5

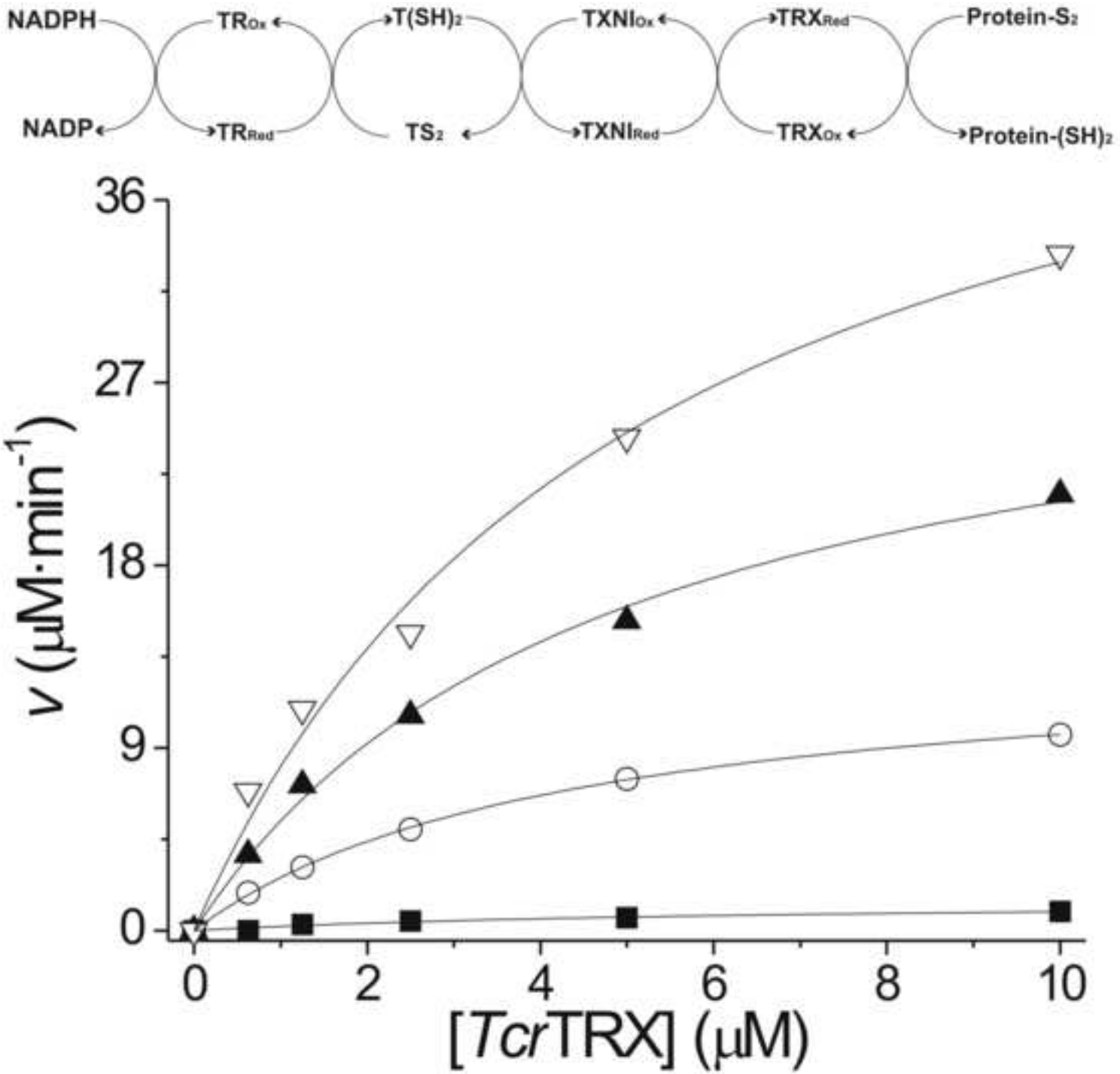

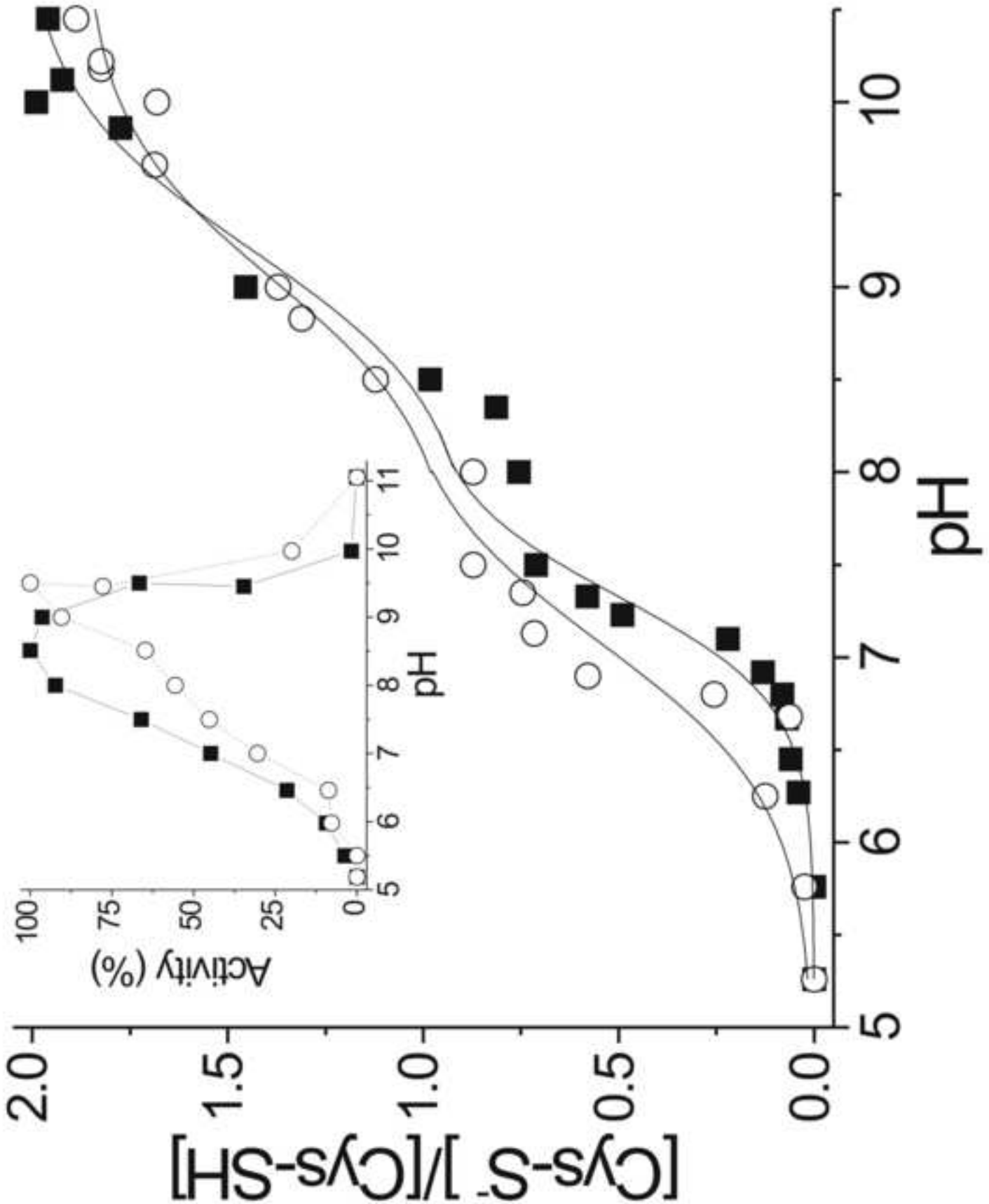
[Cys-S⁻]/[Cys-SH]
2.0
1.5
1.0
0.5
0.0
5
6
7
8
9
10
pH
Activity (%)
100
75
50
25
0
5
6
7
8
9
10
11
pH

Figure6

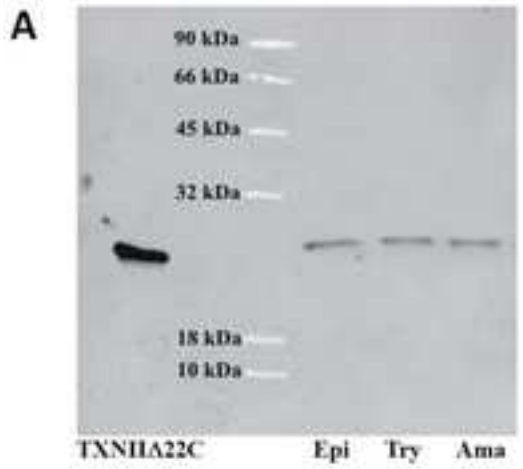

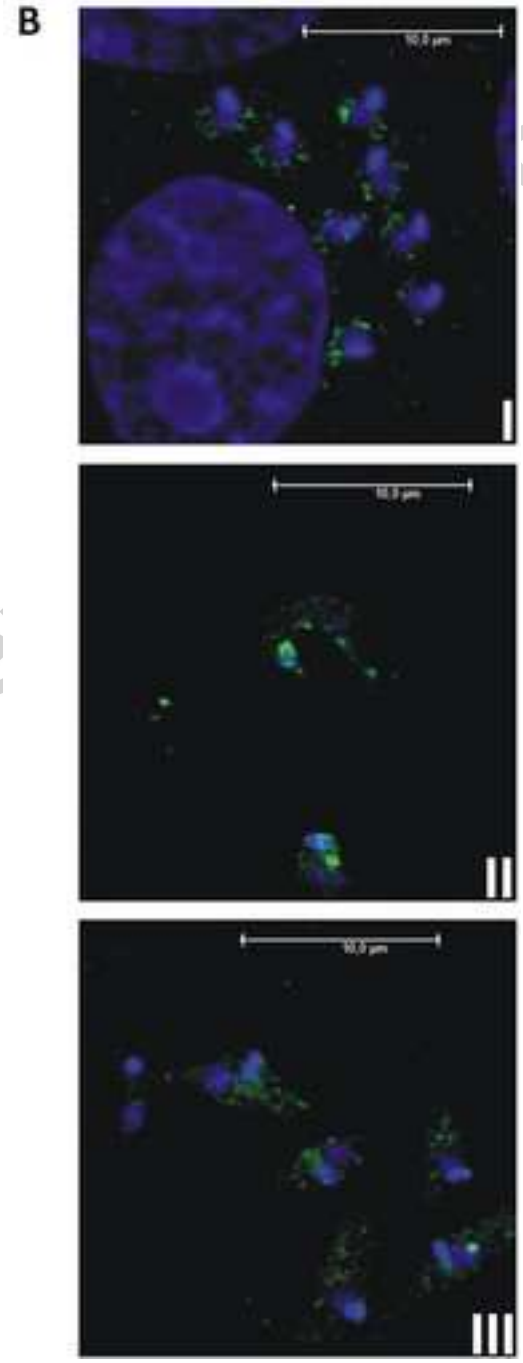

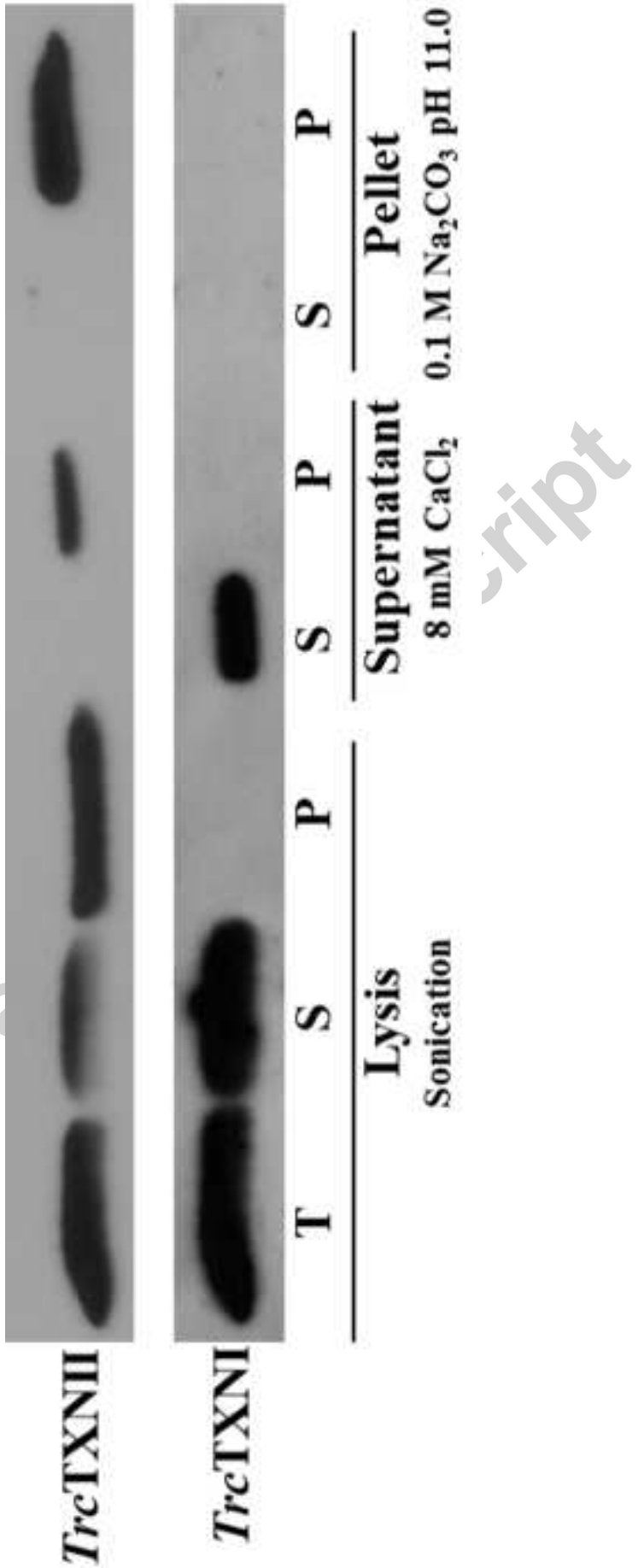

Figure8

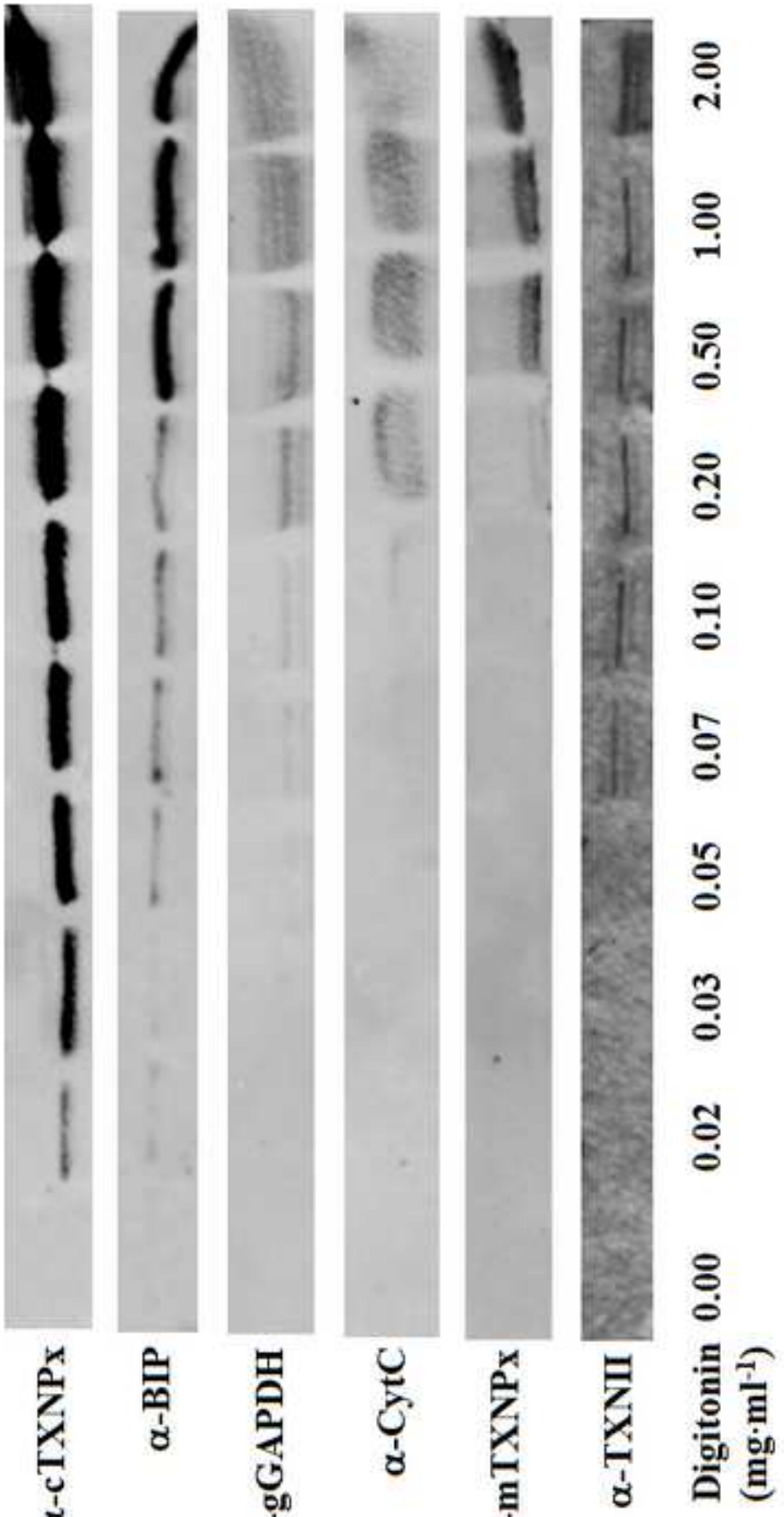

Figure9

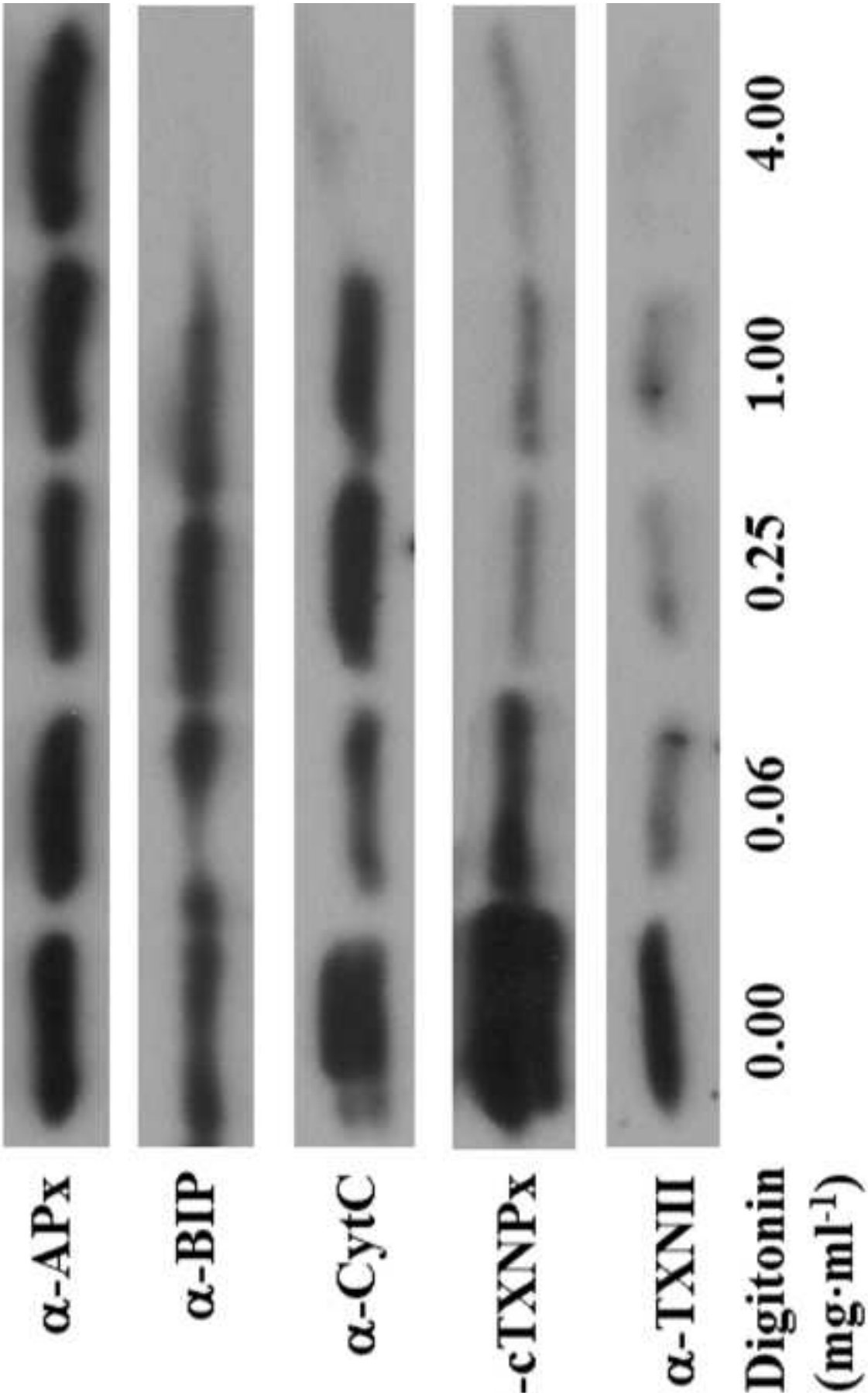

Figure10

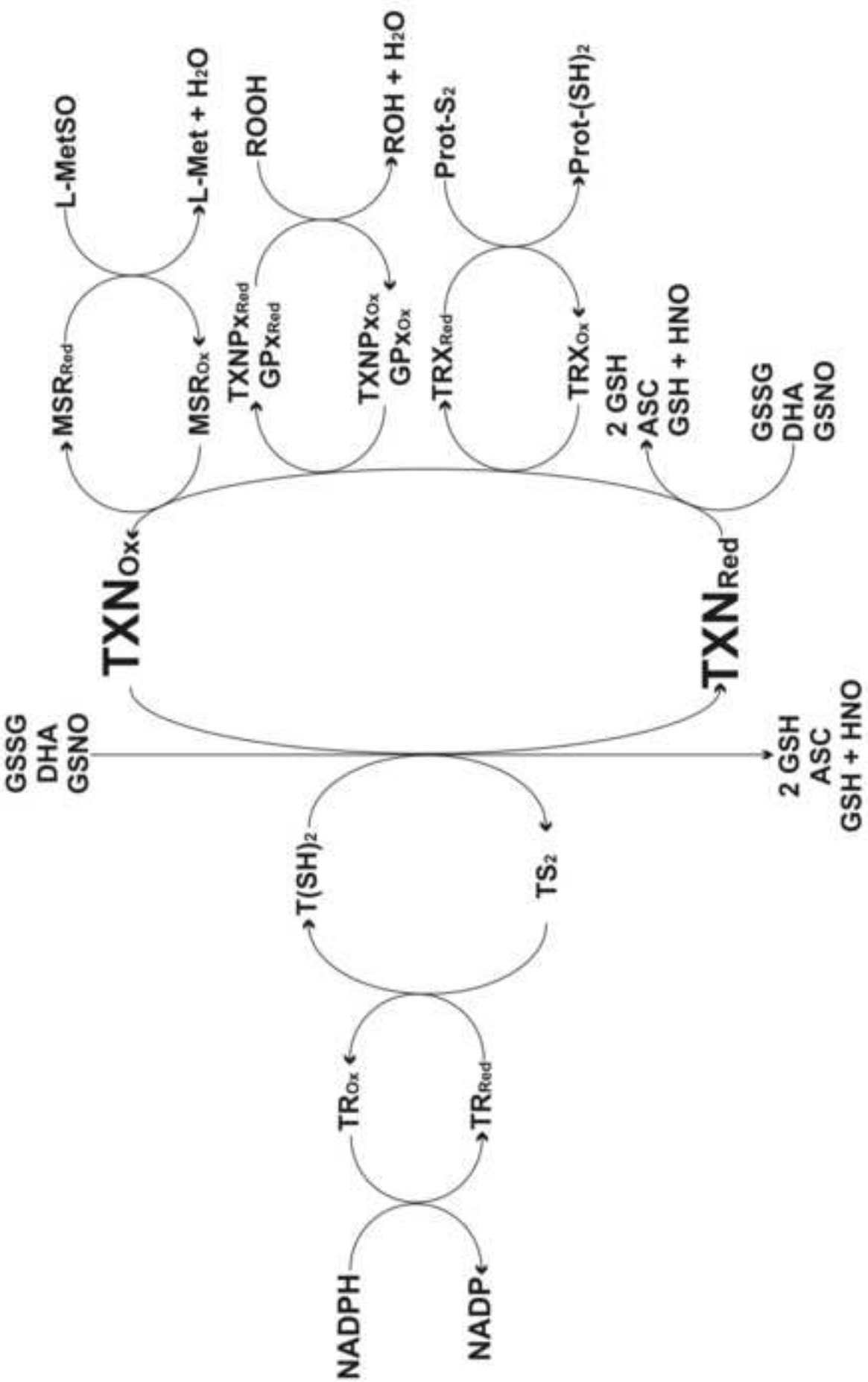
L-MetSO
L-Met + H2O
MSRRed
MSROx
ROOH
ROH + H2O
TXNPXRed
GPXRed
TXNPXOx
GPXOx
Prot-S2
Prot-(SH)2
TRXRed
TRXOx
2 GSH
ASC
GSH + HNO
GSSG
DHA
GSNO
TXNOx
TXNRed
GSSG
DHA
GSNO
2 GSH
ASC
GSH + HNO
T(SH)2
TS2
TROx
TRRed
NADPH
NADP

Figure11